THE UNIVERSITY OF CHICAGO

CURRENT-CONSTRAINED REDUCED-DENSITY-MATRIX THEORY FOR MOLECULAR CONDUCTIVITY

A DISSERTATION SUBMITTED TO
THE FACULTY OF THE DIVISION OF THE PHYSICAL SCIENCES
IN CANDIDACY FOR THE DEGREE OF
DOCTOR OF PHILOSOPHY

DEPARTMENT OF CHEMISTRY

BY
ALEXANDRA ELIZABETH RAEBER

CHICAGO, ILLINOIS
AUGUST 2020

To Colin, Elizabeth, and Michael

TABLE OF CONTENTS

LIST OF FIGURES

LIST OF TABLES

ACKNOWLEDGMENTS

First of all, I would like to thank David Mazziotti for his dedicated mentorship throughout the course of this degree. Without his advice and support, none of this work would have been possible. I'd like to thank the members of my committee, Prof. Stuart Rice and Prof. Suriyanarayanan Vaikuntanathan for their scientific advice and their willingness to work with the strangeness of a defense during a pandemic. Also, thank you to the people of the James Franck Institute who keep everything running, namely: Vera, Melinda, Brenda, Maria, and John.

Many thanks to all the members of the Mazziotti group with whom I had a chance to work over the years: Shrikant, Eric, Andrew, Romit, Charles, Chad, Erica, Valentine, Manas, Anthony, Kade, Scott, Simon, Nik, LeeAnn, Guan, Danny, Shayan, Shiva, Jason, Claire, Alison, Lexie, Olivia, and Jordan. All of you have been great co-workers and your advice on matters both scientific and not has been quite valuable. It was a pleasure to work with you all. Thank you also to my friends in the department who made my time at the University of Chicago about more than just work: Kade, Maggie, Kelliann, and Olivia.

I owe a great deal of gratitude to all of the chemistry faculty at my undergraduate alma mater, Bryn Mawr College, but especially, Prof. Susan White, Dr. Krynn Lukacs, and Prof. Michelle Francl. It was their encouragement and support that led me to pursue this degree. Thank you to my parents, Elizabeth and Michael, who have always encouraged me to follow my dreams. Lastly, thank you so much to my partner, Colin, without whose unfailing support this degree would not have been possible.

ABSTRACT

In this work, I study a variety of problems in electronic structure from a reduced density matrix perspective. In Chapter 2, I describe an extension of the current-constrained density matrix theory from its two-electron reduced density-matrix (2-RDM) formulation to a one-electron reduced density matrix (1-RDM) formulation. I demonstrate the current-constrained 1-RDM method through the computation of the theoretical, intrinsic resistance of acenes and phenacenes. In Chapter 3, I use reduced density matrix theory to study the electronic structure and conductivity of cyclo[18]carbon and its boron nitride analogue. I use the current-constrained matrix (1-RDM) theory to compute the molecular conductance in two cases: (1) conductance in the plane of the molecule and (2) conductance around the molecular ring as potentially driven by a magnetic field through the molecule's center. Off-diagonal long-range order (ODLRO) in the two-electron reduced density matrix (2-RDM) has long been recognized as a mathematical characteristic of conventional superconductors. The large eigenvalue of the 2-RDM has been shown to be a useful measure of this long-range order. In Chapter 4, I show that the cumulant 2-RDM also has a large eigenvalue in the limit of ODLRO. The largest eigenvalue of the cumulant 2-RDM is bounded from above by N. The large eigenvalue of the cumulant 2-RDM implies the large eigenvalue of the 2-RDM, and hence, is a natural measure of ODLRO that vanishes in the mean-field limit. In Chapter 5, I propose and implement a universal signature of the van der Waals interactions based on the cumulant part of the two-electron reduced density matrix (2-RDM). Due to the connected property of the cumulant, it can be used to detect the van der Waals interactions between two molecular moieties. In particular, I use the squared Frobenius norm of the cumulant of the 2-RDM, which has been previously shown to provide a size-extensive measure of the electron correlation. I study this signature of van der Waals forces in a collection of small molecules of varying geometries.

CHAPTER 1

INTRODUCTION

1.1 Wavefunction Methods

All electronic structure information about a molecule is contained in the Schrödinger equation.

$$\hat{H}\Psi_n = \hat{E}\Psi_n \tag{1.1}$$

Where $\hat{H}$ is the Hamiltonian operator, E is the energy, and Ψ_n is the wavefunction (1). This work focuses on the time-independent, electronic Schrodinger equation. The Born-Oppenheimer approximation, disregarding nuclear motion, will also be used. The resulting Hamiltonian can be broken down into two parts,

$$\hat{H} = {}^1h(i) + {}^2V(i,j), \tag{1.2}$$

where the one-body term, ${}^1h(i)$, contains the kinetic energy and electron nuclear repulsion and the two-body term,${}^2V(i,j)$, is the electron-electron repulsion. It is this second term which makes the calculation of the wavefunction difficult, as it's exact solution scales exponentially with the number of electrons in the system. Approximations to the two-body term of the Hamiltonian are the primary focus of method development in electronic structure.

The most basic approximation the full electronic wavefunction is Hartree-Fock, a mean-field approximation in which the full Hamiltonian is replaced by an effective one-electron potential known as the Fock operator,

$$\hat{F} = {}^1\hat{h}_i + {}^1\hat{J}_i - {}^1\hat{K}_i, \tag{1.3}$$

where $\hat{J}_i$ and $\hat{K}_i$ are the Coulomb and exchange operators, respectively. Together, $\hat{J}_i$ and $\hat{K}_i$, describe the average field of all other electrons felt by electon i. The Hartree-Fock

wavefunction is given by

$$|\Psi_{HF}\rangle = \frac{1}{\sqrt{N!}} \begin{vmatrix} \chi_1(1) & \dots & \chi_N(1) \\ \vdots & & \vdots \\ \chi_N(1) & \dots & \chi_N(N) \end{vmatrix} \tag{1.4}$$

where N is the number of electrons and χ_i are the set of orthonormal molecular orbitals which are generated from an optimal linear combination of the atomic orbitals. The Hartree-Fock solution is an upper-bound on the ground-state energy of the sytem, that is, it underestimates the stability of the molecule. Since no explicit two-body terms are included in the Fock operator, electron correlation is neglected in Hartree-Fock; however, this method still recovers ninety to ninety-nine percent of the full energy, depending upon the level of electron correlation present in the system. For this reason, as well as the favorable $O(r^3)$ scaling of modern implementations, we chose the Hartree-Fock as the basis for the one-electron current-constrained molecular conductivity method.

Even though correlation accounts for only a small percentage of the full energy, it plays an important role in the electronic structure of many molecules. A number of methods exist for the approximation of the two-body term of the Hamiltonian, but the most fundamental of these is configuration interaction (2). Where the Hartree-Fock wavefunction contains only a single electron configuration which corresponds to filling the ground state orbitals from most to least stable while taking into account the Pauli Exclusion principle, the configuration interaction wavefunction contains all possible electron configurations. Each of the these configurations has a weight, which is determined by variational minimization. Configuration interaction gives an exact solution to the Schrodinger equation in the limit of the basis set used. Unfortunately, this method scales expontnetially with system size, with the number of configurations given by,

$$c = \frac{2S+1}{r+1}\binom{r+1}{N/2-1}\binom{r+1}{N/2+S+1},$$

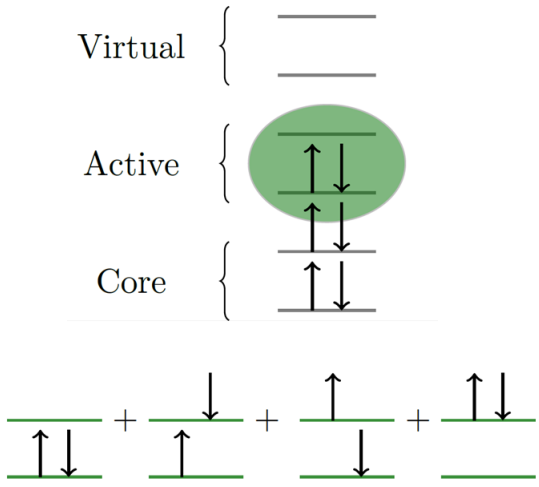

Figure 1.1: Top: An example of an active space of two electrons in two orbitals for a system with six electrons and six orbitals, with the active space highlighted in green. Bottom: A full configuration of the active space.

where N, r, and S are the number of electrons, the number of orbitals and the total spin, respectively. As a result, the current system size limit for a full configuration calculation is twenty electrons in twenty orbitals (3). Efforts to expand the usability of configuration interaction have resulted in the development of active space methods,of which a visual example is shown in Fig. 1.1. These methods consider all configurations for only a subset of the total number of electrons and orbitals in the molecule and use a more approximate method like Hartree-Fock for the rest.

1.2 Reduced Density Matrix Methods

While most electronic structure methods focus on the wavefunction, the work described in this thesis uses primarily density matrix based methods, which use the N-electron density matrix,

$$D(123..N;\bar{1}\bar{2}\bar{3}..\bar{N}) = \sum_i w_i \Psi_i(123..N)\Psi_i^*(\bar{1}\bar{2}\bar{3}..\bar{N}), \tag{1.5}$$

in place of the wavefunction. The N-electron Hamilitonian contains only two-body interactions, and electrons are indistinguishable particles, so it is possible to determine the full energy of an N-electron system from the two-electron reduced density matrix (2-RDM) without loss of information (4; 5; 6; 7). The exact energy is given by

$$E = Tr({}^2K\,{}^2D), \tag{1.6}$$

where ${}^2K$ is the reduced Hamiltonian,

$${}^2K = N\left(\frac{-\nabla^2}{2} - \sum_j \frac{Z_j}{r_{1j}}\right) + \frac{N(N-1)}{2r_{12}} \tag{1.7}$$

and ${}^2D$ is the two-electron RDM obtained by integrating the N-electron density matrix over all electrons except two,

$${}^2D(1,2;\bar{1},\bar{2}) = \int D(123..N;\bar{1}\bar{2}3..N)d3..dN. \tag{1.8}$$

As this is a much smaller object than the full wavefunction, it can be directly calculated with polynomial rather than exponential scaling (8). Care needs to be taken; however, to ensure that reduced density matrices correspond to the N-electron system in question. Additional constraints, known as N-representability conditions, must be imposed upon them (9; 10). Some of the constraints are analogous to those required in wavefunction calculations; the reduced density matrix must be antisymmetric, Hermitian, and have a normalizable trace while others are unique. An important subset of these for the 2-RDM are the 2-positivity conditions,

$${}^2D \succeq 0 \tag{1.9}$$

$${}^2Q \succeq 0 \tag{1.10}$$

$${}^2G \succeq 0 \tag{1.11}$$

where ${}^2D$, ${}^2Q$, and ${}^2G$ and the two-particle, two-hole, and particle-hole reduced density matrices respectively and $M \succeq 0$ indicates that the matrix M is positive semidefinite, that is, it has only nonnegative eigenvalues (11; 12; 13; 14). The energy in Eq. 1.6 can be obtained via variational minimization of the 2-RDM subject to the conditions given in Eqs. 1.11 through the use of a special type of convex optimization known as semidefinite programming (15; 16; 17; 18; 19; 20; 21; 22). Using the 2-positivity conditions, this method scales as $O(r^6)$, making it applicable to a wide variety of molecular systems (23; 24; 25).

1.3 Molecular Conductivity

The eventual goal of research in molecular conductivity is the creation of electronic devices in which single molecules are the basic component. Single molecules being the smallest possible electronic components, their use could theoretically result in dramatically decreased chip sizes. The idea was originally suggested by Aviram and Ratner's theoretical description of a molecular diode nearly fifty years ago (26). Since that time, a great deal of experimental and theoretical work has been devoted to the discovery of molecules which can be used as switches, wires, diodes, and transistors (27; 28; 29). The conductance of single molecules is most commonly measured by break-junction experiments, as illustrated by Fig. 1.2. A layer of the target molecule deposited on a gold substrate is contacted by the tip of a scanning tunneling microscope (STM) and a constant voltage is applied. The resulting current flow is measured as the STM tip is drawn away from the surface, creating a fully stretched metal-molecule-metal junction just before the circuit is broken. This process is repeated hundreds of times to account for non-optimal junctions (30).

Theoretical studies of molecular conductivity generally consider the entire junction, electrode and molecule, using density functional theory (DFT) to approximate the non-equilibrium Green's functions. In these calculations, the Hamiltonian of the system is par-

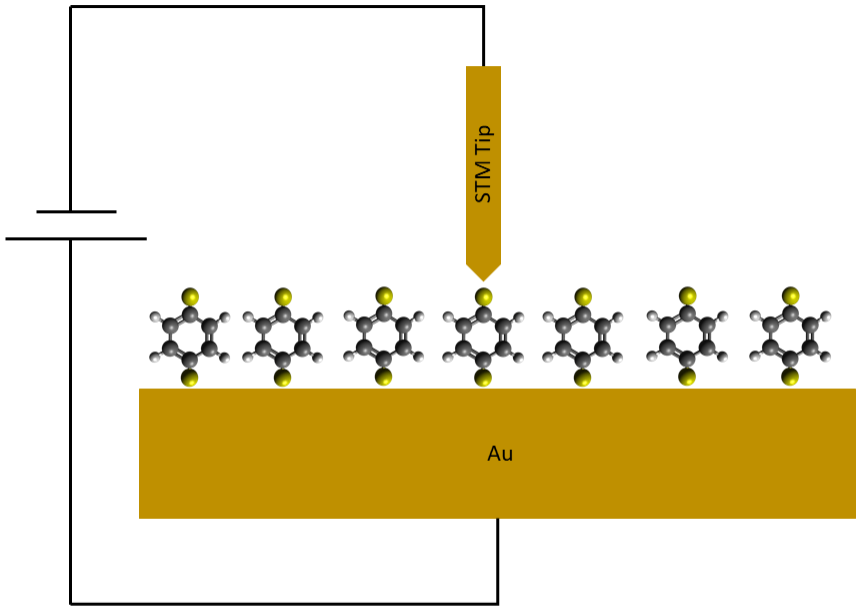

Figure 1.2: A cartoon of an STM break-junction experiment measuring the current flow through 1,4-benzenedithiol.

titioned as

$$\begin{bmatrix} H_L & H_{LM} & 0 \\ H_{LM}^{\dagger} & H_M & H_{RM}^{\dagger} \\ 0 & H_{MR} & H_R, \end{bmatrix} \tag{1.12}$$

where $H_{L(R)}$ corresponds to the left (right) electrode, H_M to the molecule, and H_{LM} and H_{MR} to the coupling between the electrode and the molecule. The Green's functions for each of these pieces are used to calculate the transmission function $T(E)$ for the molecule, which is related to the conductance by

$$G = \frac{2e^2}{\hbar} T(E). \tag{1.13}$$

The transmission function can also be used to calculate the current voltage characteristics via

$$I(V) = \int dE T(E)(f(E-\mu_R) - f(E-\mu_L)) \tag{1.14}$$

where $\mu_{R(L)}$ is the chemical potential of the left (right) electrode (31; 32). Just as in experiment, this method sets a particular voltage on the system and determines the resulting current flow. In Chapter 2 I discuss a different theoretical method for the study of single molecule conductance, the current-constrained reduced-density-matrix theory.

1.4 References

[1] Szabo, A. & Ostlund, N. S. *Modern Quantum Chemistry: Introduction to Advanced Electronic Structure Theory* (Dover Publications, 1996).

[2] Helgaker, T., Jorgensen, P. & Olsen, J. *Molecular Electronic-Structure Theory* (Wiley, 2000).

[3] Levine, D. S. *et al.* Casscf with extremely large active spaces using the adaptive sampling configuration interaction method. *J. Chem. Theor. Comput.* **16**, 2340–2354 (2020).

[4] Garrod, C. & Percus, J. K. Reduction of the n-particle variational problem. *J. Math. Phys.* **5**, 1756–1776 (1964).

[5] Mazziotti, D. A. 3, 5-contracted schrödinger equation: Determining quantum energies and reduced density matrices without wave functions. *Int. J. Quantum Chem.* **70**, 557–570 (1998).

[6] Mazziotti, D. A. Contracted schrödinger equation: Determining quantum energies and two-particle density matrices without wave functions. *Phys. Rev. A* **57**, 4219 (1998).

[7] Mazziotti, D. A. Two-electron reduced density matrix as the basic variable in many-electron quantum chemistry and physics. *Chem. Rev.* **112**, 244–262 (2012).

[8] Mazziotti, D. A. (ed.) *Reduced-density-matrix mechanics: with application to many-electron atoms and molecules*, vol. 134 (John Wiley & Sons, 2007).

[9] Coleman, A. J. Structure of fermion density matrices. *Rev. Mod. Phys.* **35**, 668 (1963).

[10] Coleman, A. J. & Yukalov, V. I. *Reduced density matrices: Coulson's challenge*, vol. 72 (Springer Science & Business Media, 2000).

[11] Erdahl, R. M. Representability. *Int. J. Quantum Chem.* **13**, 697–718 (1978).

[12] Kummer, H. n-representability problem for reduced density matrices. *J. Math. Phys.* **8**, 2063–2081 (1967).

[13] Mazziotti, D. A. & Erdahl, R. Uncertainty relations and reduced density matrices: mapping many-body quantum mechanics onto four particles. *Phys. Rev. A* **63**, 042113 (2001).

[14] Zhao, Z., Braams, B. J., Fukuda, M., Overton, M. L. & Percus, J. K. The reduced density matrix method for electronic structure calculations and the role of three-index representability conditions. *J. Chem. Phys.* **120**, 2095–2104 (2004).

[15] Nakata, M. *et al.* Variational calculations of fermion second-order reduced density matrices by semidefinite programming algorithm. *J. Chem. Phys.* **114**, 8282 (2001).

[16] Mazziotti, D. A. variational minimization of atomic and molecular ground-state energies via the two-particle reduced density. *Phys. Rev. A* **65**, 062511 (2002).

[17] Mazziotti, D. A. First-order semidefinite programming for the direct determination of two-electron reduced density matrices with application to many-electron atoms and molecules. *J. Chem. Phys.* **121**, 10957–10966 (2004).

[18] Mazziotti, D. A. Realization of quantum chemistry without wave functions through first-order semidefinite programming. *Phys. Rev. Lett.* **93**, 213001 (2004).

[19] Mazziotti, D. A. Variational reduced-density-matrix method using three-particle n-representability conditions with application to many-electron molecules. *Phys. Rev. A* **74**, 032501 (2006).

[20] Mazziotti, D. A. First-order semidefinite programming for the two-electron treatment of many-electron atoms and molecules. *ESAIM: Math. Modell. Numer. Anal.* **41**, 249 (2007).

[21] Gidofalvi, G. & Mazziotti, D. A. Active-space two-electron reduced-density-matrix method: Complete active-space calculations without diagonalization of the n-electron hamiltonian. *J. Chem. Phys.* **129**, 134108 (2008).

[22] Shenvi, N. & Izmaylov, A. F. Active-space n-representability constraints for variational two-particle reduced density matrix calculations. *Phys. Rev. Lett.* **105**, 213003 (2010).

[23] Schlimgen, A. W. & Mazziotti, D. A. Static and dynamic electron correlation in the ligand noninnocent oxidation of nickel dithiolates. *J. Phys. Chem. A* **121**, 9377–9384 (2017).

[24] McIsaac, A. R. & Mazziotti, D. A. Ligand non-innocence and strong correlation in manganese superoxide dismutase mimics. *Phys. Chem. Chem. Phys.* **19**, 4656–4660 (2017).

[25] Montgomery, J. M. & Mazziotti, D. A. Strong electron correlation in nitrogenase co-factor, FeMoco. *J. Phys. Chem. A.* **122**, 4988–4996 (2018).

[26] Aviram, A. & Ratner, M. A. Molecular rectifiers. *Chem. Phys. Lett.* **29**, 277–283 (1974).

[27] Xiang, D., Wang, X., Jia, C., Lee, T. & Guo, X. Molecular-scale electronics: from concept to function. *Chem. Rev.* **116**, 4318–4440 (2016).

[28] Mathew, P. T. & Fang, F. Advances in molecular electronics: a brief review. *Engineering* **4**, 760–771 (2018).

[29] Xin, J., N.and Guan *et al.* Concepts in the design and engineering of single-molecule electronic devices. *Nature Rev. Phys.* **1**, 211–230 (2019).

[30] Komoto, Y., Fujii, S., Iwane, M. & Kiguchi, M. Single-molecule junctions for molecular electronics. *J. Mat. Chem. C* **4**, 8842–8858 (2016).

[31] Taylor, J., Guo, H. & Wang, J. Ab initio modeling of quantum transport properties of molecular electronic devices. *Phys. Rev. B* **63**, 245407 (2001).

[32] Yongqiang, X., Supriyo, D. & Ratner, M. A. First-principles based matrix green's function approach to molecular electronic devices: general formalism. *Chem.Phys.* **281**, 151 – 170 (2002).

CHAPTER 2

CURRENT-CONSTRAINED ONE-ELECTRON REDUCED DENSITY-MATRIX THEORY FOR NON-EQUILIBRIUM STEADY-STATE MOLECULAR CONDUCTIVITY

Reprint with permission from A. E. Raeber and D. A. Mazziotti, *Phys. Chem. Chem. Phys.* **21** 12620 (2019).

2.1 Introduction

When Aviram and Ratner suggested the possibility of a single molecule diode in 1974 (1), the concept of molecular-scale electronics was entirely theoretical. The development of single molecule measurement techniques(2; 3) made the testing of such components an experimental reality (4; 5). Since then, a number of molecules have been found to function as molecular wires (6), switches (7; 8), and diodes (9; 10). Current theoretical studies generally use density functional theory (DFT) (11; 12; 13; 14; 15; 16; 17; 18) or reduced density matrix (RDM) theory (19; 20) to approximate the non-equilibrium Green's functions. Just as in experiment, these methods calculate the current flow through a system which results from setting a particular bias voltage.

Recent work proposed a different paradigm to study single molecule conductance, the current-constrained reduced-density-matrix theory. This method imposes a current on the molecule and measures the bias voltage required to generate the current-constrained non-equilibrium steady state. In the previous work, the current constraint is added to a variational minimization of the 2-electron reduced-density-matrix or 2-RDM (21). Here, we extend the theory to a one-electron reduced density matrix (1-RDM) form. The 1-RDM,

$$^1D(1:\bar{1}) = \int {}^N D(1,...N;\bar{1},...N) d2..dN, \tag{2.1}$$

which is obtained by integrating the N-particle density matrix over all particles save one, contains all the information needed to study one-electron properties. By analogy with the 2-RDM stationary-state (22; 23; 24; 25; 26; 27; 28; 29; 30; 31; 32; 33; 34; 35; 36; 37; 38; 39) and steady-state work (21), we perform a variational minimization of the energy of the molecule as a functional of the 1-RDM which is subject to the N-representability conditions (40; 41; 34; 42), ensuring that the 1-RDM represents at least one N-electron density matrix, but also a current constraint that sets the average current fluxing through the molecule. The 1-RDM current-constrained theory is compatible with any one-electron electronic structure theory including Hartree-Fock, density functional (43; 44), and tight-binding (45; 46) methods. While the 1-RDM method does not include an explicit description of electron correlation, it provides a qualitatively correct description of single molecule conductivity at low computational cost.

After deriving the current-constrained 1-RDM method in section 2.2, we apply it in section 2.3 to compute the steady-state, intrinsic resistance of the acenes and phenacenes in the Hartree-Fock approximation as a function of their length. The intrinsic resistance of a molecule is its resistance to the flow of electrons along a chosen direction where the current is added to the isolated molecule as a constraint. Both acenes and phenacenes exhibit trends in their intrinsic resistance that reflect trends in available experimental data (47).

2.2 Theory

To define a 1-RDM theory of molecular conductivity, we begin with variational principle in the absence of electron transport. The energy of the system, given by

$$E = \mathrm{Tr}({}^1K^1D), \tag{2.2}$$

is minimized subject to N-representability conditions known as the 1-positivity constraints, which ensure that the 1-RDM generated in the minimization arises from the integration of

at least one N-electron density matrix (40; 41; 48; 49; 50). These conditions have the form,

$$^1D \succeq 0 \tag{2.3}$$

$$^1Q \succeq 0 \tag{2.4}$$

where ^1D and ^1Q are the one-particle and one-hole reduced density matrices and the symbol $\succeq$ indicates that they must remain positive semidefinite, that is, they must have nonnegative eigenvalues.

To set the current for the system, we define the one-electron current matrix as the matrix representation of the one-electron gradient in a specified direction $\hat{\kappa}$, given by

$$^1J_q^p = \frac{1}{L}\int_{dr} \phi_p(r)(\nabla \cdot \hat{\kappa})\phi_q(r)dr, \tag{2.5}$$

where L is the length of the molecule, r represents the electronic coordinates, and $\hat{\kappa}$ is the vector direction of the current, and ϕ_p are the molecular orbitals (21). We add this to the energy minimization by requiring that

$$\mathrm{Tr}(^1J\ \mathrm{Im}(^1D)) = I, \tag{2.6}$$

where ^1J is given above. This method of energy minimization is a special type of convex optimization known as semidefinite programming (SDP) (27; 26; 32; 34). The current constraint generates a complex-valued SDP that can be mapped to a real-valued SDP by representing the complex matrix M by a larger real-valued matrix S,

$$S = \begin{pmatrix} \mathrm{Re}(M) & \mathrm{Im}(M) \\ -\mathrm{Im}(M) & \mathrm{Re}(M). \end{pmatrix} \tag{2.7}$$

The S matrix is positive semidefinite if and only if the M matrix is positive semidefinite.

Solving this semidefinite program generates the reorganization energy due to the current

constraint. Since charge polarization is the microscopic starting point for conductivity, we follow Ref. (21) in assuming that the energetic response ΔE_{curr} of a molecule to a current constraint is comparable to its energetic response ΔE_{field} to an electric field ϵ applied in the same direction,

$$\Delta E_{\text{curr}} \approx \Delta E_{\text{field}} = \alpha\epsilon^2 = \alpha\frac{V^2}{L^2}, \tag{2.8}$$

where L is the length of the molecule and α is its electric field polarizability. Solving for the voltage V, we obtain the following formula (21) for V in terms of ΔE_{curr}, L, and α

$$V \approx L\left(\frac{\Delta E_{\text{curr}}}{\alpha}\right)^{1/2}. \tag{2.9}$$

This estimated voltage and the current set in Eq. (2.6) can then be used to compute the conductance (or resistance) of the system.

2.3 Applications

Graphene (51), and its acene precursors (52), are of particular interest in the field of molecular electronics. Recently, linear acenes have been used to create stable and highly conductive molecular junctions at room temperature, without the need for thiol linkers between the molecule and the metal leads (53). In this work, we calculate the response energy and voltage of linear acene and phenacene chains, shown in Fig. 1, of three to seven phenyl rings in length over a current range of 0 to 20 μA, where the current is applied in the direction of chain growth. We generate the Hamiltonian from the Fock matrix from a minimization of the Hartree-Fock energy of each molecule at the 631-G level of theory. Since we are interested in a qualitative description of the conductivity which arises only from the molecule itself, we compute the intrinsic conductance of the molecule, omitting the thiol linkers and metal leads.

For a given number of phenyl rings, acenes require a lower voltage than phenacenes to support a given current, indicating that as a whole acenes have higher conductivity than

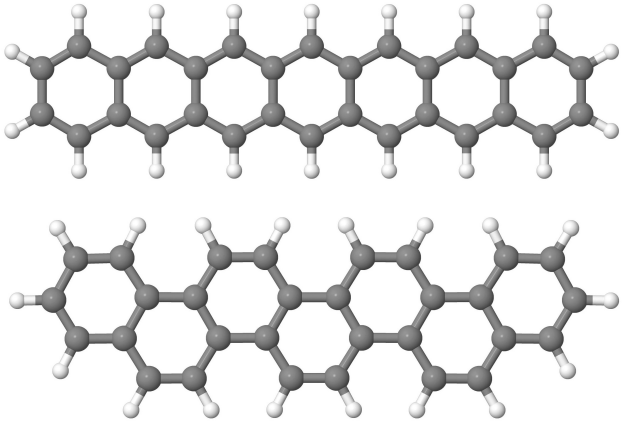

Figure 2.1: Ball and stick representations of 7-acene (top) and 7-phenacene (bottom)

the corresponding phenacenes, as shown by the current-voltage plots for the acenes and phenacenes in Fig. 2. While phenacenes have a lower reorganization energy at a particular current, their lower electric field polarizability results in a higher voltage requirement. For both the acenes and the phenacenes the voltage necessary to achieve a particular current is directly proportional to chain length, as has been shown in experiment for the acenes (47).

In single molecule junctions, conductance has been shown experimentally to decay exponentially with the length of the molecule as given by

$$G \propto e^{-\beta L} \tag{2.10}$$

where β is the decay constant and L is the length of the molecule (54). To determine the length dependence of conductance in the acene chains, we calculate the current through the atomic orbitals of the atoms of the edge rings of each acene

$$\tilde{I} = \mathrm{Tr}({}^1\tilde{J}\mathrm{Im}({}^1D)), \tag{2.11}$$

where

$$\tilde{J} = C_{MO}^{AO} P J \tag{2.12}$$

in which P is the projector onto selected orbitals at the edge of each acene. When this edge

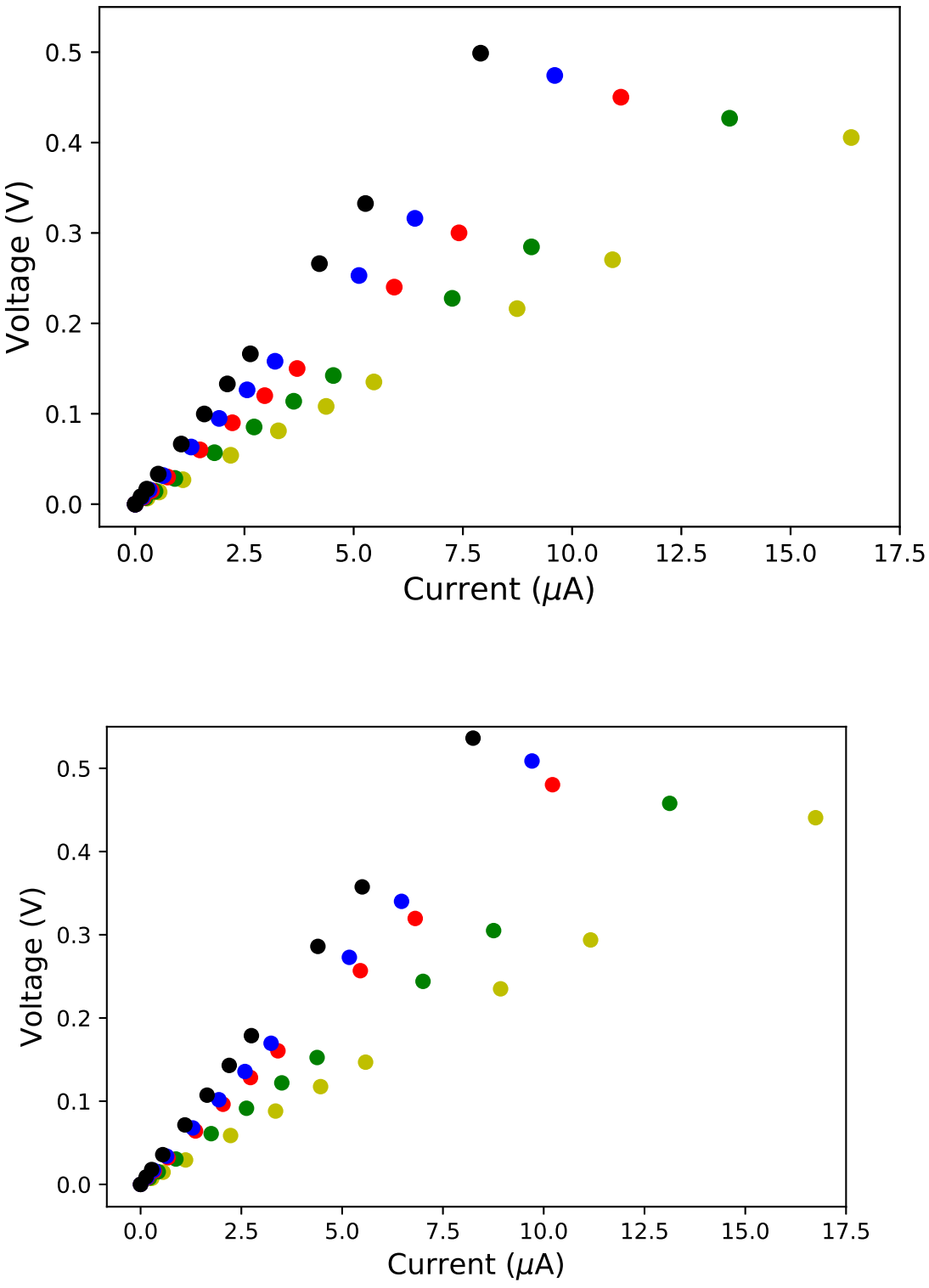

Figure 2.2: Current plotted as a function of voltage for the N-acenes (top) and N-phenacenes (bottom), where N is 3 (yellow), 4 (green), 5 (red), 6 (blue), and 7 (black).

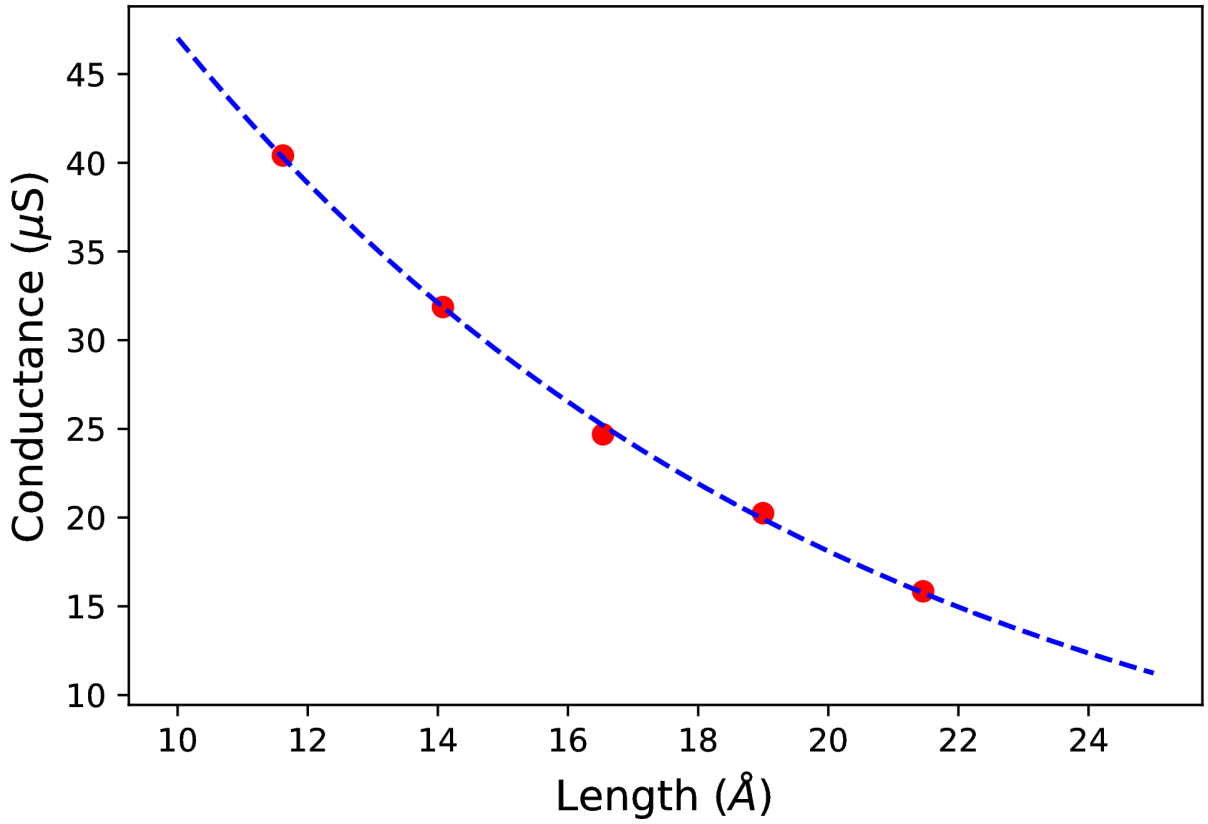

Figure 2.3: Molecular conductance plotted as a function of length for 3-acene through 7-acene (red). In all cases, the current is set to 0.662 μA and the atomic orbitals selected are those of the 12 carbons and 8 hydrogens in the outermost phenyl ring on each end of the molecule. A least-squares exponential fit with a β value of 0.009568 1/Å is shown in blue.

current rather than the average current is used to calculate the conductance, we recover the expected exponential decay, as shown in Fig. 3, indicating that the edge behavior of single molecules can be seen without including explicit leads in the calculation.

2.4 Discussion and Conclusions

In this work we extend the current-constrained reduced-density-matrix theory for non-equilibrium, steady-state molecular conductivity from its original 2-RDM formulation to a 1-RDM formulation. We show that, like the 2-RDM version, this formulation gives ohmic current-voltage relationships in the low bias region and captures the tunneling effect in the

edge conductance of the linear acenes. This method achieves a qualitatively correct description of the length dependence of conductivity in the linear acenes. We also find that linear aromatic chains of phenyl rings are more effective conductors than alternating aromatic chains.

Traditional theories of molecular conductivity add a voltage to the molecule to compute the current. In the current-constrained RDM theories the current is added as a constraint to compute the reorganization energy and the voltage. This change in paradigm allows us to compute an intrinsic resistance (or conductance) for each molecule that depends only upon a molecule's energetic response to the imposed current constraint as well as its intrinsic properties such as length and polarization. Importantly, as shown in the results, the intrinsic resistance reflects key qualitative features of molecular conductivity, features that are determined mainly by the electronic properties of the molecule. Even the exponential decay in the edge current, observed experimentally in acene chains, is qualitatively captured by the current-constrained computation of each chain's intrinsic resistance. The computation of intrinsic resistance provides a useful metric by which to compare the intrinsic capacity of molecules and materials for efficient electron transport.

While in this work, we use Hartree-Fock theory to generate the Hamiltonian, the theory can be interfaced with other one-electron-based electronic structure methods, including DFT and semi-empirical tight binding methods. The current-constrained 1-RDM theory provides a qualitatively correct description of single molecule conductivity at low computational cost.

2.5 References

[1] Aviram, A. & Ratner, M. A. Molecular rectifiers. *Chem. Phys. Lett.* **29**, 277–283 (1974).

[2] Binnig, G. & Rohrer, H. Scanning tunneling microscopy. *Surf. Sci.* **126**, 236–244 (1983).

[3] Binnig, G., Quate, C. F. & Gerber, C. Atomic force microscope. *Phys. Rev. Lett.* **56**, 930–933 (1986).

[4] Xu, B. & Tao, N. J. Measurement of single-molecule resistance by repeated formation of molecular junctions. *Science* **301**, 1221–1223 (2003).

[5] Lang, K. *et al.* Conducting atomic force microscopy for nanoscale tunnel barrier characterization. *Rev. Sci. Instrum.* **75**, 2726–2731 (2004).

[6] Tour, J. M. *et al.* Synthesis and preliminary testing of molecular wires and devices. *Chem. Eur. J.* **7**, 5118–5134 (2001).

[7] Chen, J., Reed, M. A., Rawlett, A. M. & Tour, J. M. Large on-off ratios and negative differential resistance in a molecular electronic device. *Science* **286**, 1550–1552 (1999).

[8] Ismael, A. K. *et al.* Side-group-mediated mechanical conductance switching in molecular junctions. *Angew. Chem. Int. Ed.* **56**, 15378–15382 (2017).

[9] Capozzi, B. *et al.* Single-molecule diodes with high rectification ratios through environmental control. *Nat. Nanotechnol.* **10**, 522 (2015).

[10] Batra, A. *et al.* Tuning rectification in single-molecular diodes. *Nano Lett.* **13**, 6233–6237 (2013).

[11] Taylor, J., Guo, H. & Wang, J. Ab initio modeling of quantum transport properties of molecular electronic devices. *Phys. Rev. B* **63**, 245407 (2001).

[12] Damle, P. S., Ghosh, A. W. & Datta, S. Unified description of molecular conduction: From molecules to metallic wires. *Phys. Rev. B* **64**, 201403 (2001).

[13] Di Ventra, M. & Lang, N. D. Transport in nanoscale conductors from first principles. *Phys. Rev. B* **65**, 045402 (2001).

[14] X., Y., D., S. & Ratner, M. A. First-principles based matrix green's function approach to molecular electronic devices: general formalism. *Chem.Phys.* **281**, 151 – 170 (2002).

[15] Brandbyge, M., Mozos, J.-L., Ordejón, P., Taylor, J. & Stokbro, K. Density-functional method for nonequilibrium electron transport. *Phys. Rev. B* **65**, 165401 (2002).

[16] Varga, K. Time-dependent density functional study of transport in molecular junctions. *Phys. Rev. B* **83**, 195130 (2011).

[17] Hsu, L.-Y. & Rabitz, H. Single-molecule phenyl-acetylene-macrocycle-based optoelectronic switch functioning as a quantum-interference-effect transistor. *Phys. Rev. Lett.* **109**, 186801 (2012).

[18] Hsu, L.-Y., Jin, B.-Y., Chen, C.-H. & Peng, S.-M. Reaction: New insights into molecular electronics. *Chem* **3**, 378 – 379 (2017).

[19] Rothman, A. E. & Mazziotti, D. A. Nonequilibrium, steady-state electron transport with n-representable density matrices from the anti-hermitian contracted schrödinger equation. *J. Chem. Phys.* **132**, 104112 (2010).

[20] Hoy, E. P., Mazziotti, D. A. & Seideman, T. Development and application of a 2-electron reduced density matrix approach to electron transport via molecular junctions. *J. Chem. Phys.* **147**, 184110 (2017).

[21] Sajjan, M. & Mazziotti, D. A. Current-constrained density-matrix theory to calculate molecular conductivity with increased accuracy. *Commun. Chem. (Nature)* **1**, 31 (2018).

[22] Mazziotti, D. A. Two-electron reduced density matrix as the basic variable in many-electron quantum chemistry and physics. *Chem. Rev.* **112**, 244 (2012).

[23] Mazziotti, D. A. & Erdahl, R. Uncertainty relations and reduced density matrices: mapping many-body quantum mechanics onto four particles. *Phys. Rev. A: At., Mol., Opt. Phys.* **63**, 042113 (2001).

[24] Nakata, M. *et al.* Variational calculations of fermion second-order reduced density matrices by semidefinite programming algorithm. *J. Chem. Phys.* **114**, 8282 (2001).

[25] Mazziotti, D. A. variational minimization of atomic and molecular ground-state energies via the two-particle reduced density. *Phys. Rev. A* **65**, 062511 (2002).

[26] Zhao, Z., Braams, B. J., Fukuda, M., Overton, M. L. & Percus, J. K. The reduced density matrix method for electronic structure calculations and the role of three-index representability conditions. *J. Chem. Phys.* **120**, 2095 (2004).

[27] Mazziotti, D. A. Realization of quantum chemistry without wave functions through first-order semidefinite programming. *Phys. Rev. Lett.* **93**, 213001 (2004).

[28] Cances, E., Stoltz, G. & Lewin, M. The electronic ground-state energy problem: a new reduced density matrix approach. *J. Chem. Phys.* **125**, 064101 (2006).

[29] Mazziotti, D. A. Variational reduced-density-matrix method using three-particle n-representability conditions with application to many-electron molecules. *Phys. Rev. A* **74**, 032501 (2006).

[30] Mazziotti, D. A. First-order semidefinite programming for the two-electron treatment of many-electron atoms and molecules. *ESAIM: Math. Modell. Numer. Anal.* **41**, 249 (2007).

[31] Shenvi, N. & Izmaylov, A. F. Active-space n-representability constraints for variational two-particle reduced density matrix calculations. *Phys. Rev. Lett.* **105**, 213003 (2010).

[32] Mazziotti, D. A. Large-scale semidefinite programming for many-electron quantum mechanics. *Phys. Rev. Lett.* **106**, 083001 (2011).

[33] Verstichel, B., van Aggelen, H., Poelmans, W. & Van Neck, D. Variational two-particle density matrix calculation for the hubbard model below half filling using spin-adapted lifting conditions. *Phys. Rev. Lett.* **108**, 213001 (2012).

[34] Mazziotti, D. A. Structure of fermionic density matrices: Complete n-representability conditions. *Phys. Rev. Lett.* **108**, 263002 (2012).

[35] Fosso-Tande, J., Nguyen, T.-S., Gidofalvi, G. & DePrince, A. E. Large-scale variational two-electron reduced-density-matrix-driven complete active space self-consistent field methods. *J. Chem. Theory Comput.* **12**, 2260 (2016).

[36] Mazziotti, D. A. Enhanced constraints for accurate lower bounds on many-electron quantum energies from variational two-electron reduced density matrix theory. *Phys. Rev. Lett.* **117**, 153001 (2016).

[37] Montgomery, J. M. & Mazziotti, D. A. Strong electron correlation in nitrogenase co-factor, FeMoco. *J. Phys. Chem. A.* **122**, 4988–4996 (2018).

[38] Safaei, S. & Mazziotti, D. A. Quantum signature of exciton condensation. *Phys. Rev. B.* **98**, 045122 (2018).

[39] Schlimgen, A. W. & Mazziotti, D. A. Analytical gradients of variational reduced-density-matrix and wavefunction-based methods from an overlap-reweighted semidefinite program. *J. Chem. Phys.* **149**, 164111 (2018).

[40] Coleman, A. J. Structure of fermion density matrices. *Rev. Mod. Phys.* **35**, 668–686 (1963).

[41] Coleman, A. J. & Yukalov, V. I. *Reduced density matrices: Coulson's challenge*, vol. 72 (Springer Science & Business Media, 2000).

[42] Veeraraghavan, S. & Mazziotti, D. A. Semidefinite programming formulation of linear-scaling electronic structure theories. *Phys. Rev. A* **92**, 022512 (2015).

[43] Parr, R. G. & Yang, W. *Density-functional theory of atoms and molecules*, vol. 16 (Oxford University Press, 1989).

[44] Jones, R. O. Density functional theory: Its origins, rise to prominence, and future. *Rev. Mod. Phys.* **87**, 897–923 (2015).

[45] Sutton, A. P., Finnis, M. W., Pettifor, D. G. & Ohta, Y. The tight-binding bond model. *J. Phys. C* **21**, 35 (1988).

[46] Elstner, M. & Seifert, G. Density functional tight binding. *Phil. Trans. R. Soc. A* **372**, 20120483 (2014).

[47] Kim, B., Seong Ho Choi, S.-H., Zhu, X.-Y. & Frisbie, C. D. Molecular tunnel junctions based on π-conjugated oligoacene thiols and dithiols between ag, au, and pt contacts: effect of surface linking group and metal work function. *J. Am. Chem. Soc.* **133**, 19864–19877 (2011).

[48] Piris, M. Global method for electron correlation. *Phys. Rev. Lett.* **119**, 063002 (2016).

[49] Benavides-Riveros, C. L. & Schilling, C. Natural extension of hartree–fock through extremal 1-fermion information: overview and application to the lithium atom. *Z. Phys. Chem.* **230**, 703–717 (2016).

[50] Schilling, C. Relating the pure and ensemble density matrix functional. *J. Chem. Phys.* **149**, 231102 (2018).

[51] Jung, I., Dikin, D. A., Piner, R. D. & Ruoff, R. S. Tunable electrical conductivity of individual graphene oxide sheets reduced at "low" temperatures. *Nano Lett.* **8**, 4283–4287 (2008).

[52] Gidofalvi, G. & Mazziotti, D. A. Active-space two-electron reduced-density-matrix method: Complete active-space calculations without diagonalization of the n-electron hamiltonian. *J. Chem. Phys.* **129**, 134108 (2008).

[53] Liu, C., Kaneko, S., Komoto, Y., Fujii, S. & Kiguchi, M. Highly conductive single

naphthalene and anthracene molecular junction with well-defined conductance. *App. Phys. Lett.* **106**, 103103 (2015).

[54] Metzger, R. M. Unimolecular electronics. *Chem. Rev.* **115**, 5056–5115 (2015).

CHAPTER 3

NON-EQUILIBRIUM STEADY STATE CONDUCTIVITY IN CYCLO[18]CARBON AND ITS BORON NITRIDE ANALOGUE

This chapter is reprinted from a paper submitted for publication by A.E. Raeber and D. A. Mazziotti.

3.1 Introduction

The structure and properties of ring-shaped carbon allotropes, known as cyclo[n]carbons, have been of theoretical interest for many years, first appearing in the literature more than fifty years ago (1). As a result of their sp hybridization, cyclo[n]carbons have two orthogonal π systems, allowing for the possibility of double aromatic stabilization (2; 3). Their high reactivity, however, means that their synthesis was not possible until very recently. Last year, the first of these carbon allotropes, cyclo[18]carbon, was synthesized and characterized using high-resolution atomic force microscopy (4).

Prior to its synthesis, two possible structures had been hypothesized for cyclo[18]carbon, a cumulenic form, without bond length alternation, and a polyynic form, with alternating single and triple bonds. The cumulenic structure, which is predicted by Hückel theory, is generally found to be the lowest in energy by density functional theory (DFT) (5; 6; 7) and Møller-Plesset second-order perturbation theory (8) calculations. The polyynic structure, on the other hand is supported by Hartree-Fock (9; 10), Monte-Carlo (11), and coupled cluster calculations (12). Recent experimental work confirmed the polyynic geometry to be correct (4; 13; 14).

Boron nitride (BN) forms hexagonal lattices which are isoelectric to those formed by carbon. Its two-dimensional hexagonal lattice is analogous to graphene and has high thermal and chemical stability (15). Theoretical work on boron nitride analogues to cyclo[n]carbons has shown that they may have similar novel properties with higher stability (16; 17; 18).

Here we study the electronic structure and molecular conductivity of the cyclo[18]carbon and B_9N_9 molecules using reduced density matrix (RDM) theory (19; 20; 21; 22; 23; 24; 25). Computations with the variational two-electron reduced density matrix (2-RDM) method (19; 20; 21; 22; 23), which can treat fractionally filled orbitals and strong electron correlation if present (26; 27; 28), reveal that neither molecule is strongly correlated and support the experimental polyynic structure of cyclo[18]carbon. Using a current-constrained 1-electron reduced density matrix (1-RDM) theory with the Hartree-Fock molecular orbitals and energies (24; 25), we compute the intrinsic molecular conductance of both molecules in two cases: (1) conductance in the plane of the molecule and (2) conductance around the molecular ring as potentially driven by a magnetic field through the molecule's center.

We find for both cyclo[18]carbon and B_9N_9 that conductance in the plane of the molecule is greater than conductance around the ring. Furthermore, cyclo[18]carbon is slightly more conductive than B_9N_9 for both (1) and (2). The intrinsic conductance provides information about the intrinsic ability of a molecule to support conductance that does not consider the resistance from the junction or lead. Intrinsic conductance is useful for assessing whether a molecule is a potentially good molecular conductor or insulator prior to optimization of the lead and/or junction. The conductance per molecular orbital is also obtained, providing insight into how the orbitals—their energies and densities—drive the conduction.

3.2 Theory

The idea of creating single molecule circuit elements has been of scientific interest for nearly fifty years (29), with a great deal of progress being made in the past twenty years (30; 31; 32). Traditional theories of molecular conductivity add a voltage to the molecule to compute the current (33; 34; 35; 36; 37; 38; 39; 40; 41; 42). In the current-constrained RDM theories the current is added as a constraint to compute the reorganization energy and the voltage (24; 25). This change in paradigm allows us to compute an intrinsic conductance (or resistance) for each molecule that depends only upon a molecule's energetic response to the

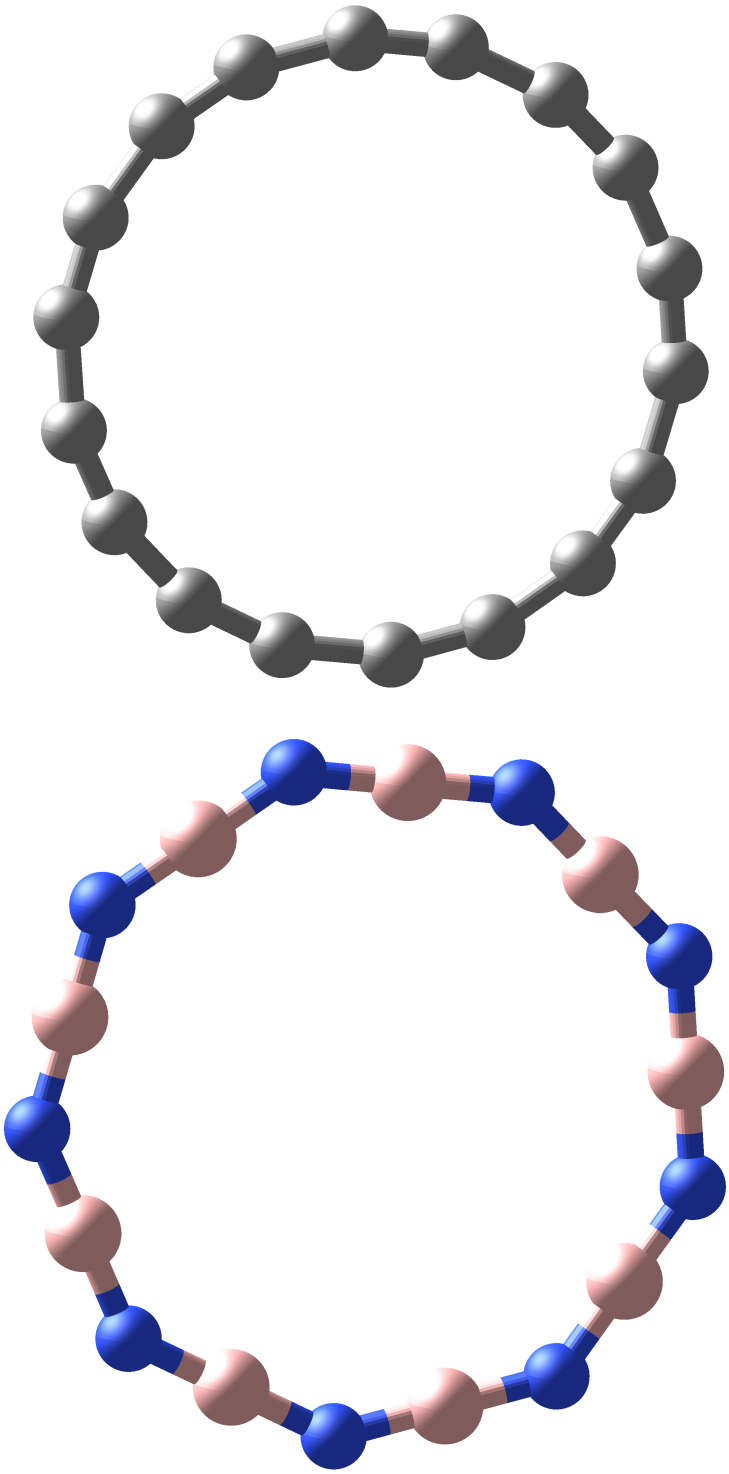

Figure 3.1: Ball and stick representations of C_{18} (top) and B_9N_9 (bottom)

imposed current constraint, as well as its intrinsic properties such as length and polarization. The intrinsic resistance reflects key qualitative features of molecular conductivity, features that are determined mainly by the electronic properties of the molecule.

To define a 1-RDM theory of molecular conductivity, we begin with the variational principle in the absence of electron transport. The energy of the system, given by

$$E = \mathrm{Tr}({}^1K\,{}^1D), \tag{3.1}$$

where ${}^1K$ is the matrix form of the one-electron reduced Hamiltonian, which we approximate as the Fock matrix and ${}^1D$ is the 1-RDM. This energy is minimized subject to ensemble N-representability conditions on the 1-RDM known as the 1-positivity constraints, which ensure that the 1-RDM generated in the minimization arises from the integration of at least one N-electron ensemble density matrix (43; 44; 23; 45; 46; 47). These conditions have the form,

$${}^1D \succeq 0 \tag{3.2}$$

$${}^1Q \succeq 0 \tag{3.3}$$

where ${}^1D$ and ${}^1Q$ are the one-particle and one-hole reduced density matrices and the symbol $\succeq$ indicates that they must remain positive semidefinite, that is, they must have non-negative eigenvalues. These conditions are equivalent to the Pauli exclusion principle, which restricts the occupation of each spin orbital to lie between 0 and 1. This method of energy minimization is a special type of convex optimization known as semidefinite programming (SDP) (20; 48; 22; 23).

To set the current for the system, we define the one-electron current matrix as the matrix representation of the one-electron gradient in a specified direction $\hat{\kappa}$, given by

$${}^1J_q^p = \frac{1}{L}\int_{dr} \phi_p(r)(\nabla \cdot \hat{\kappa})\phi_q(r)dr, \tag{3.4}$$

where L is the length of the molecule, r represents the electronic coordinates, $\hat{\kappa}$ is the vector direction of the current, and ϕ_p are the molecular orbitals (24). We add this to the energy minimization by requiring that

$$\mathrm{Tr}({}^1J\ \mathrm{Im}({}^1D)) = I, \tag{3.5}$$

where I is the current.

In order to investigate the conductivity in the ring rather than across it, changes are made to the form of the one-electron current matrix. For the ring current calculations,

$${}^1\tilde{J}^p_q = \left(\sum_i^M L^{-1} \int_{dr} \phi_p(r)(\nabla \cdot \hat{\kappa_i})\phi_q(r)dr\right) M^{-1}, \tag{3.6}$$

where M is the number of atoms in the ring and κ_i is the unit vector tangent to the center of each atom.

3.3 Results and Discussion

3.3.1 Electronic Structure

Molecular geometries of C_{18} and B_9N_9 as shown in Fig. 3.1 are obtained by optimization at the v2RDM-CASSCF/cc-pVDZ level of theory (49; 19; 20; 21; 22; 23) with an active space of 18 electrons in 18 orbitals, implemented in the Quantum Chemistry Package (50) in Maple (51). The v2RDM method predicts the experimental polyynic structure, with alternating carbon-carbon bond lengths of 1.50 Å and 1.22 Å. The calculated structure of B_9N_9 agrees well with the DFT structure from recent previous work (18), with a boron-nitrogen bond length of 1.32 Å.

One of the key features of C_{18} is its dual π system, which is well represented in the v2RDM results, with π-type active molecular orbitals which lie either in the plane of the molecule or perpendicular to it. A representative subset of the active orbitals is shown in Fig. 3.4. Our calculations indicated that this dual π system is shared by B_9N_9, with a

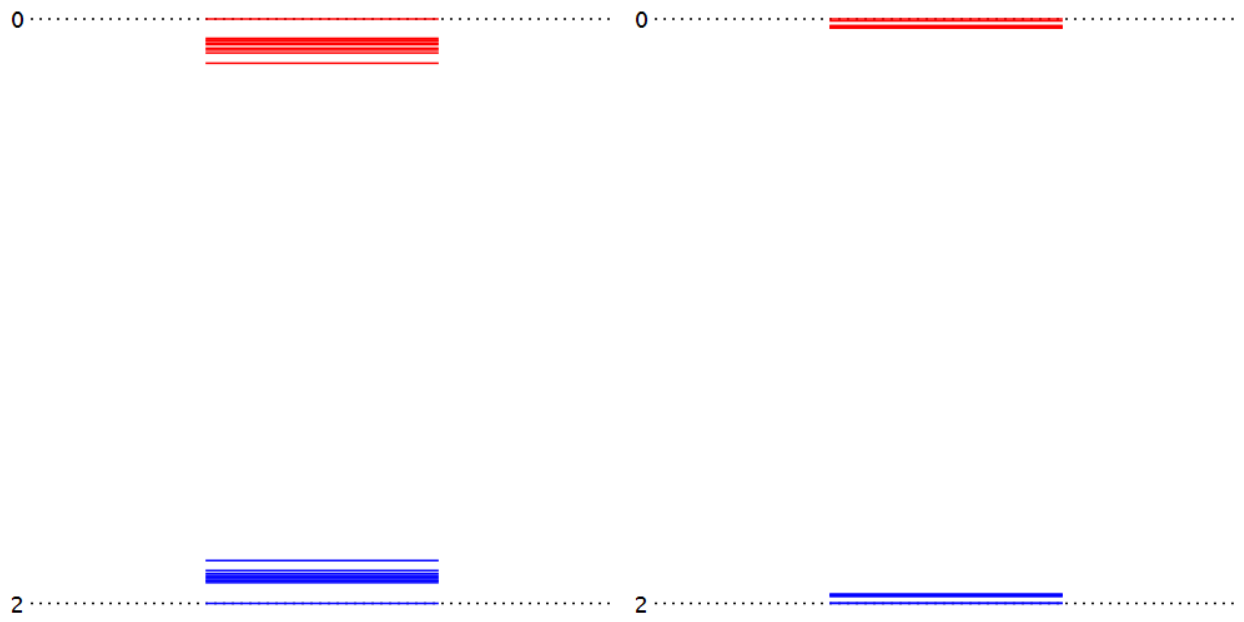

Figure 3.2: NO occupations of C_{18} (left) and B_9N_9 (right)

representative subset shown in Fig. 3.5.

We also find that these molecules do not have a high level of static correlation. The natural orbital occupations in the active space, as shown in Fig. 3.2, do not diverge much from a completely filled (2) or empty (0) state. The occupation of the highest occupied natural orbital (HONO) is 1.85 and the occupation of the lowest unoccupied natural orbital (LUNO) is 0.15. B_9N_9 displays even less static correlation than C_{18}, with a occupation of 1.97 in the HONO and occupation of 0.03 in the LUNO. The minimal static correlation in these molecules supports the computation of their molecular conductivity within a 1-RDM theory.

3.3.2 Molecular Conductivity

We investigate the conductance both around the molecular ring and in the plane of the molecule for cyclo[18]carbon and B_9N_9. All molecules are centered at the origin and the vector direction $\hat{\kappa}$ of the current is set as the x-axis for the calculation of the in-plane current and as described in the theory section for the ring current. We generate the Hamiltonian

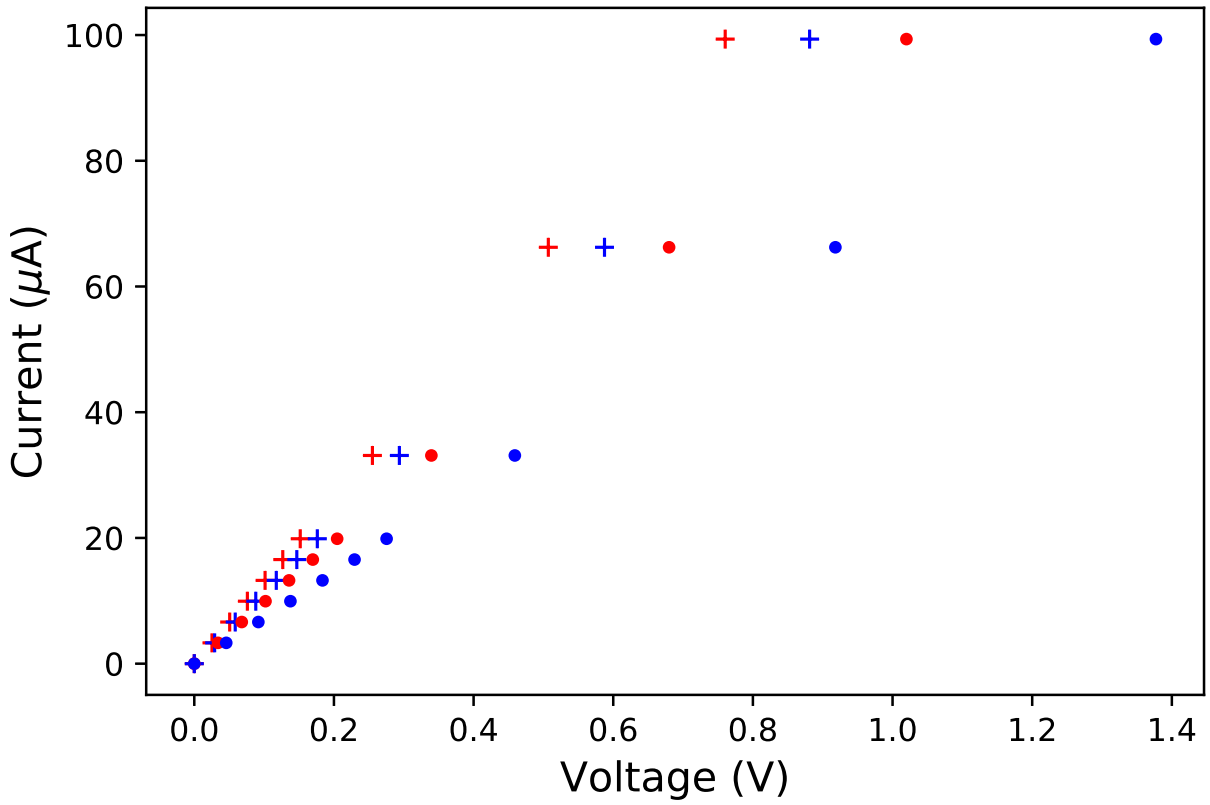

Figure 3.3: Voltage plotted as a function of current for C_{18} ring (red circle), C_{18} in-plane (red plus), B_9N_9 ring (blue circle), B_9N_9 in-plane (blue plus).

using the Fock matrix from a minimization of the Hartree-Fock energy of each molecule in the cc-pVDZ basis set. Since we are interested in a qualitative description of the conductivity which arises only from the molecule itself, we compute the intrinsic conductance of the molecule, omitting the thiol linkers and metal leads present in an experimental molecular junction.

As shown in Fig. 3.3 we find that cyclo[18]carbon is the more conductive of the two molecules, with a ring conductance of 97.42 μS and a in-plane conductance of 130.64 μS compared to a ring conductance of 72.14 μS and a in-plane conductance of 112.73 μS for B_9N_9. The lower conductance of B_9N_9 is expected based on its larger energy gap between the highest occupied molecular orbital (HOMO) and the lowest unoccupied molecular orbital (LUMO), with a gap of 13.28 eV compared to the 2.97 eV gap for C_{18}. While experimental

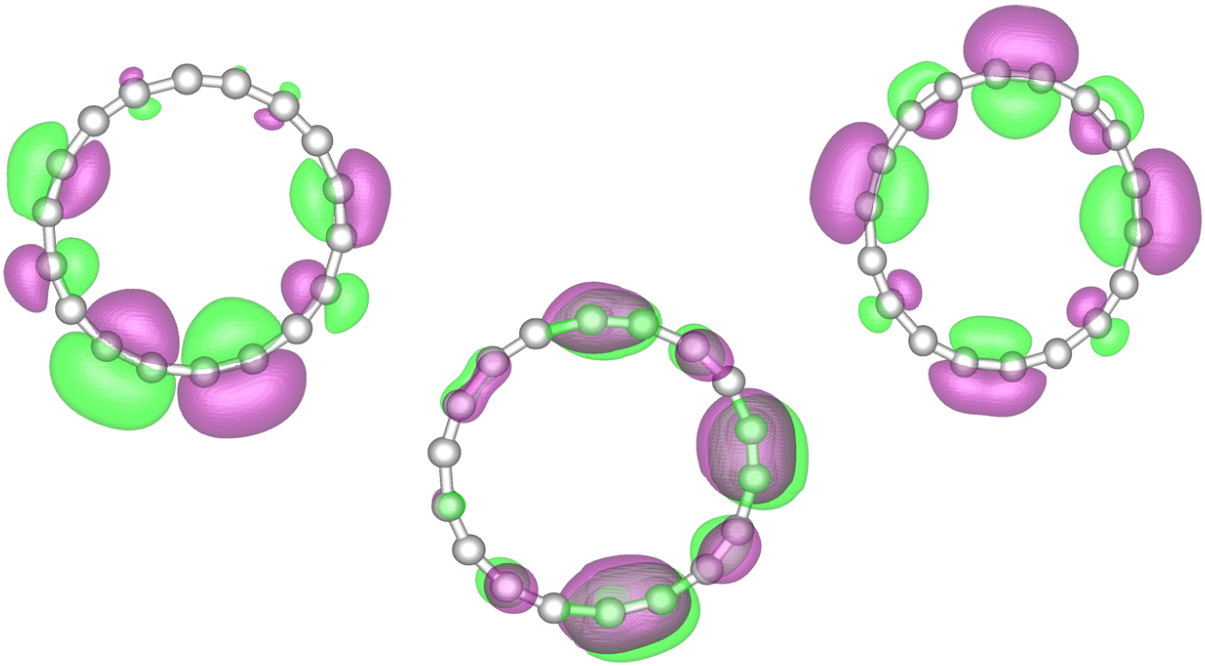

Figure 3.4: A sample of the active space molecular orbitals for C_{18}

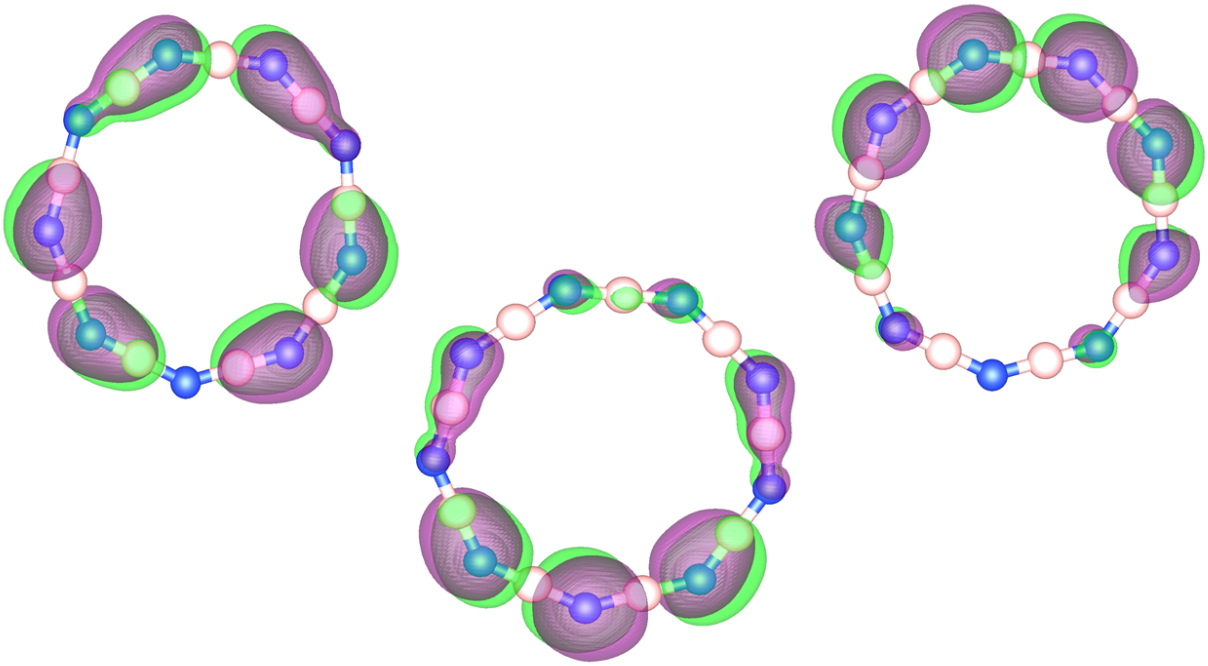

Figure 3.5: A sample of the active space molecular orbitals for B_9N_9

conductance values for these molecules are not available, the conductance of cyclo[18]carbon does agree well with that recently calculated using an NEGF-DFT method (52). For both molecules, the in-plane conductance through the center of the molecule is greater than the ring conductance.

We are also able to investigate the conductance per molecular orbital for the molecules in question, as shown in Fig. 3.6. For both molecules a small number of molecular orbitals near the HOMO-LUMO gap are the most involved in conductance. Ten percent of the orbitals contain thirty-nine percent of the current in C_{18} and thirty-seven percent of the current in B_9N_9. These orbitals are a mix of π and σ orbitals which are symmetric or nearly symmetric. The core orbitals and the high-energy virtual orbitals are much less involved in conductance than those near the Fermi level, with the core orbitals carrying on average an order of magnitude less current and the high-energy virtual orbitals carrying as much as four orders of magnitude less current. While implementations of many traditional theories like NEGF-DFT require the selection of an energy range for the conductivity, the current-constrained RDM theory predicts the energy (orbital) channels that support the molecular conductivity.

3.4 Conclusions

In the current-constrained 1-RDM theory the current is added as a constraint to compute the voltage, the opposite of traditional theories, which impose a voltage on the molecule to compute the resulting current. As a result of this change in paradigm, we compute an intrinsic conductance for each molecule, a quantity which depends only upon a molecule's energetic response to the imposed current and its electronic structure. As shown in the results, the intrinsic conductance provides a good starting point for the determination of molecular species which may be useful for molecular electronic applications, as molecules without good intrinsic conductance will not be good experimental conductors.

The current-constrained RDM theory also allows for the study of facets of the conductiv-

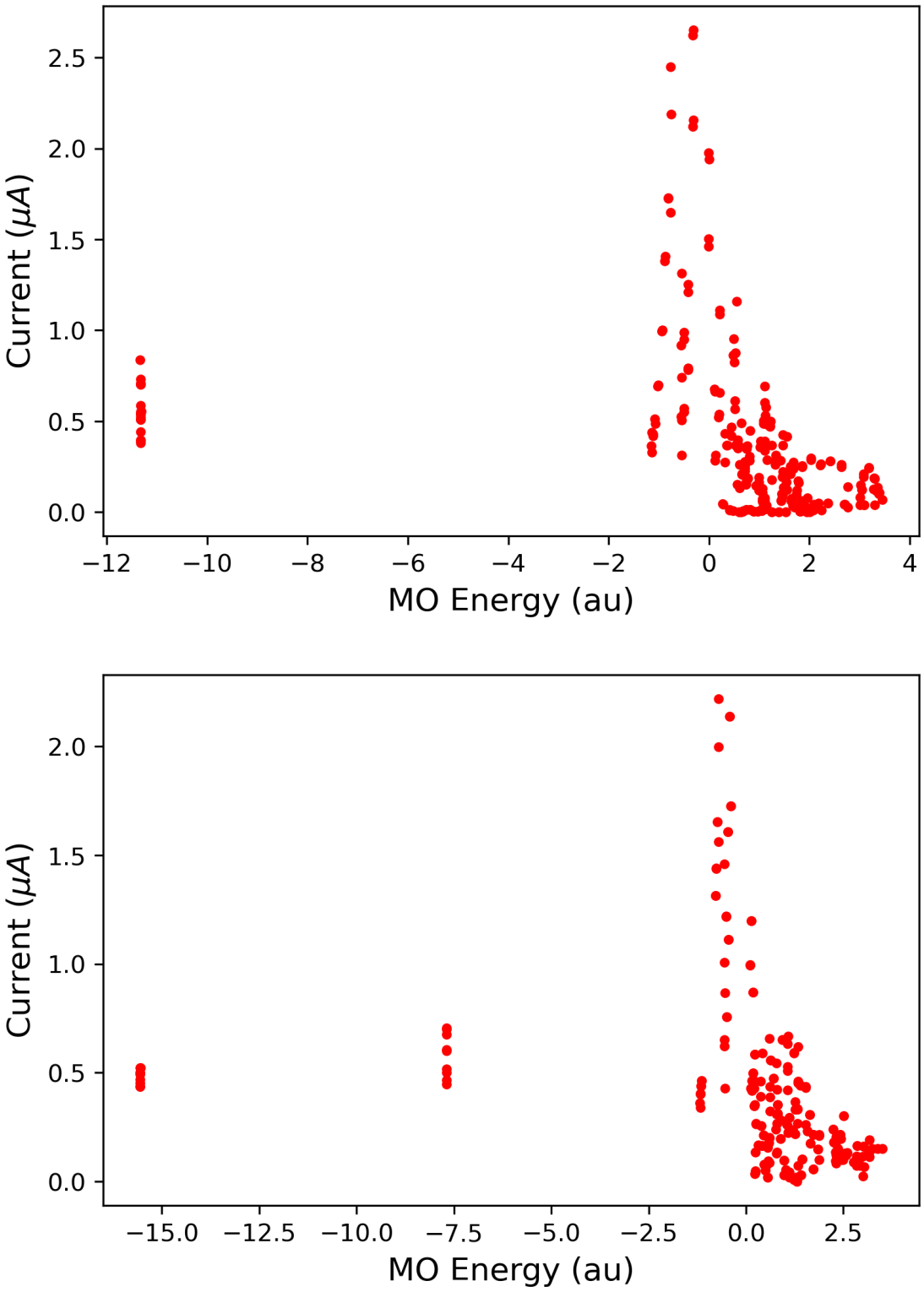

Figure 3.6: Current per MO as a function of MO energy for C_{18} (top) and B_9N_9 (bottom). In both cases a total of 100 μA of current is imposed on the system.

ity which are not easily accessible using traditional theories, including the ring conductance and the orbital and energy localization of the current. The direct computation of the 1-RDM allows us to construct the equivalent of a molecular-orbital diagram in molecular conductivity where the conductance of each orbital is presented as a function of energy. Just a molecular-orbital diagrams provide an intuitive picture for molecular bonding, these molecular-orbital conduction diagrams provide an intuitive picture for molecular conductivity.

In the this work we investigate the electronic structure of cyclo[18]carbon and its boron nitride analogue using the v2RDM-CASSCF method. We find that the molecular geometry of C_{18} obtained from v2RDM optimization agrees with that found in a recent experiment, and that the key features of its electronic structure are well-described. We apply the current-constrained theory for molecular conductivity to study the ring and in-plane conductivity of these molecules. We find that they have higher in-plane conductivity than ring conductivity and that C_{18} is more conductive than B_9N_9.

3.5 References

[1] Hoffmann, R. Extended hückel theory—v: Cumulenes, polyenes, polyacetylenes and cn. *Tetrahedron* **22**, 521–538 (1966).

[2] Fowler, P. W., Mizoguchi, N., Bean, D. E. & Havenith, R. W. A. Double aromaticity and ring currents in all-carbon rings. *Chem. Eur. J.* **15**, 6964–6972 (2009).

[3] Baryshnikov, G. V., Valiev, R. R., Kuklin, A. V., Sundholm, D. & Ågren, H. Cyclo [18] carbon: Insight into electronic structure, aromaticity, and surface coupling. *J. Phys. Chem. Lett.* **10**, 6701–6705 (2019).

[4] Kaiser, K. *et al.* An sp-hybridized molecular carbon allotrope, cyclo [18] carbon. *Science* **365**, 1299–1301 (2019).

[5] Hutter, J., Luethi, H. P. & Diederich, F. Structures and vibrational frequencies of the carbon molecules c_2-c_{18} calculated by density functional theory. *J. Am. Chem. Soc.* **116**, 750–756 (1994).

[6] Saito, M. & Okamoto, Y. Second-order jahn-teller effect on carbon $4n+2$ member ring clusters. *Phys. Rev. B* **60**, 8939 (1999).

[7] Neiss, C., Trushin, E. & Görling, A. The nature of one-dimensional carbon: Polyynic versus cumulenic. *Chem. Phys. Chem* **15**, 2497–2502 (2014).

[8] Parasuk, V., Almlof, J. & Feyereisen, M. W. The [18] all-carbon molecule: Cumulene or polyacetylene? *J. Am. Chem. Soc.* **113**, 1049–1050 (1991).

[9] Diederich, F. *et al.* All-carbon molecules: evidence for the generation of cyclo[18]carbon from a stable organic precursor. *Science* **245**, 1088–1090 (1989).

[10] Plattner, D. A. & Houk, K. N. C18 is a polyyne. *J. Am. Chem. Soc.* **117**, 4405–4406 (1995).

[11] Torelli, T. & Mitas, L. Electron correlation in c_{4n+2} carbon rings: aromatic versus dimerized structures. *Phys. Rev. Lett.* **85**, 1702 (2000).

[12] Arulmozhiraja, S. & Ohno, T. Ccsd calculations on c_{14}, c_{18}, and c_{22} carbon clusters. *J. Chem. Phys.* **128**, 114301 (2008).

[13] Scriven, L. M. *et al.* Synthesis of cyclo [18] carbon via debromination of c18br6. *J. Am. Chem. Soc.* (2020).

[14] Hussain, S., Chen, H., Zhang, Z. & Zheng, H. Vibrational spectra and chemical imaging of cyclo[18]carbon by tip enhanced raman spectroscopy. *Chem. Commun.* **56**, 2336–2339 (2020).

[15] Strout, D. L. Structure and stability of boron nitrides: the crossover between rings and cages. *J. Phys. Chem A* **105**, 261–263 (2001).

[16] Martin, J. M. L., El-Yazal, J. & François, J.-P. Structure and vibrations of $b_n n_n$ (n= 3–10). *Chem. Phys. Lett.* **248**, 95–101 (1996).

[17] Giuffreda, M. G., Deleuze, M. S. & François, J.-P. Structural, rotational, and vibrational properties of mixed ionized boron-nitrogen clusters $b_n n_n{}^+$(n= 3- 10). *J. Phys. Chem. A* **104**, 5855–5860 (2000).

[18] Pichierri, F. Boron-nitrogen analogues of cyclo [18] carbon. *Chem. Phys. Lett.* **738**, 136860 (2020).

[19] Mazziotti, D. A. First-order semidefinite programming for the direct determination of two-electron reduced density matrices with application to many-electron atoms and molecules. *J. Chem. Phys.* **121**, 10957–10966 (2004).

[20] Mazziotti, D. A. Realization of quantum chemistry without wave functions through first-order semidefinite programming. *Phys. Rev. Lett.* **93**, 213001 (2004).

[21] Gidofalvi, G. & Mazziotti, D. A. Active-space two-electron reduced-density-matrix method: Complete active-space calculations without diagonalization of the n-electron hamiltonian. *J. Chem. Phys.* **129**, 134108 (2008).

[22] Mazziotti, D. A. Large-scale semidefinite programming for many-electron quantum mechanics. *Phys. Rev. Lett.* **106**, 083001 (2011).

[23] Mazziotti, D. A. Structure of fermionic density matrices: Complete n-representability conditions. *Phys. Rev. Lett.* **108**, 263002 (2012).

[24] Sajjan, M. & Mazziotti, D. A. Current-constrained density-matrix theory to calculate molecular conductivity with increased accuracy. *Commun. Chem. (Nature)* **1**, 31 (2018).

[25] Raeber, A. E. & Mazziotti, D. A. Current-constrained one-electron reduced density-matrix theory for non-equilibrium steady-state molecular conductivity. *Phys. Chem. Chem. Phys.* **21**, 12620–12624 (2019).

[26] Schlimgen, A. W., Heaps, C. W. & Mazziotti, D. A. Entangled electrons foil synthesis of elusive low-valent vanadium oxo complex. *J. Phys. Chem. Lett.* **7**, 627–631 (2016).

[27] Montgomery, J. M. & Mazziotti, D. A. Strong electron correlation in nitrogenase co-factor, femoco. *J. Phys. Chem. A* **122**, 4988–4996 (2018).

[28] Boyn, J.-N., Xie, J., Anderson, J. S. & Mazziotti, D. A. Entangled electrons drive a non-superexchange mechanism in a cobalt quinoid dimer complex. *J. Phys. Chem. Lett.* **11**, 4584–4590 (2020).

[29] Aviram, A. & Ratner, M. A. Molecular rectifiers. *Chem. Phys. Lett.* **29**, 277–283 (1974).

[30] Chen, J., Reed, M. A., Rawlett, A. M. & Tour, J. M. Large on-off ratios and negative differential resistance in a molecular electronic device. *Science* **286**, 1550–1552 (1999).

[31] Tour, J. M. *et al.* Synthesis and preliminary testing of molecular wires and devices. *Chem. Eur. J.* **7**, 5118–5134 (2001).

[32] Batra, A. *et al.* Tuning rectification in single-molecular diodes. *Nano Lett.* **13**, 6233–6237 (2013).

[33] Xiang, D., Wang, X., Jia, C., Lee, T. & Guo, X. Molecular-scale electronics: from concept to function. *Chem. Rev.* **116**, 4318–4440 (2016).

[34] Hsu, L.-Y., Jin, B.-Y., Chen, C.-H. & Peng, S.-M. Reaction: New insights into molecular electronics. *Chem* **3**, 378 – 379 (2017).

[35] Taylor, J., Guo, H. & Wang, J. Ab initio modeling of quantum transport properties of molecular electronic devices. *Phys. Rev. B* **63**, 245407 (2001).

[36] Damle, P. S., Ghosh, A. W. & Datta, S. Unified description of molecular conduction: From molecules to metallic wires. *Phys. Rev. B* **64**, 201403 (2001).

[37] Di Ventra, M. & Lang, N. D. Transport in nanoscale conductors from first principles. *Phys. Rev. B* **65**, 045402 (2001).

[38] X., Y., D., S. & Ratner, M. A. First-principles based matrix green's function approach to molecular electronic devices: general formalism. *Chem.Phys.* **281**, 151 – 170 (2002).

[39] Brandbyge, M., Mozos, J.-L., Ordejón, P., Taylor, J. & Stokbro, K. Density-functional method for nonequilibrium electron transport. *Phys. Rev. B* **65**, 165401 (2002).

[40] Varga, K. Time-dependent density functional study of transport in molecular junctions. *Phys. Rev. B* **83**, 195130 (2011).

[41] Rothman, A. E. & Mazziotti, D. A. Nonequilibrium, steady-state electron transport with n-representable density matrices from the anti-hermitian contracted schrödinger equation. *J. Chem. Phys.* **132**, 104112 (2010).

[42] Hoy, E. P., Mazziotti, D. A. & Seideman, T. Development and application of a 2-electron reduced density matrix approach to electron transport via molecular junctions. *J. Chem. Phys.* **147**, 184110 (2017).

[43] Coleman, A. J. Structure of fermion density matrices. *Rev. Mod. Phys.* **35**, 668–686 (1963).

[44] Coleman, A. J. & Yukalov, V. I. *Reduced density matrices: Coulson's challenge*, vol. 72 (Springer Science & Business Media, 2000).

[45] Piris, M. Global method for electron correlation. *Phys. Rev. Lett.* **119**, 063002 (2016).

[46] Benavides-Riveros, C. L. & Schilling, C. Natural extension of hartree–fock through extremal 1-fermion information: overview and application to the lithium atom. *Z. Phys. Chem.* **230**, 703–717 (2016).

[47] Schilling, C. Relating the pure and ensemble density matrix functional. *J. Chem. Phys.* **149**, 231102 (2018).

[48] Zhao, Z., Braams, B. J., Fukuda, M., Overton, M. L. & Percus, J. K. The reduced density matrix method for electronic structure calculations and the role of three-index representability conditions. *J. Chem. Phys.* **120**, 2095 (2004).

[49] Dunning Jr., T. H. Gaussian basis sets for use in correlated molecular calculations. i. the atoms boron through neon and hydrogen. *The Journal of chemical physics* **90**, 1007–1023 (1989).

[50] Maplesoft, a division of Waterloo Maple Inc. Quantum Chemistry Toolbox from RDM-Chem (2020).

[51] Maplesoft, a division of Waterloo Maple Inc. Maple (2020).

[52] Zhang, L., Li, H., Feng, Y. P. & Shen, L. Diverse transport behaviors in cyclo [18] carbon–based molecular devices. *J. Phys. Chem. Lett.* **11**, 2611–2617 (2020).

CHAPTER 4

LARGE EIGENVALUE OF THE CUMULANT PART OF THE TWO-ELECTRON REDUCED DENSITY MATRIX AS A MEASURE OF OFF-DIAGONAL LONG-RANGE ORDER

Reprint with permission from A. E. Raeber and D. A. Mazziotti, *Phys. Rev. A* **92**, 052502 (2015).

4.1 Introduction

Superconductivity is an important phenomenon in condensed matter physics arising from a pairing of the electrons that exhibits long-range order (1; 2; 3). Both Yang (4) and Sasaki (5; 6) showed that this long-range order, called off-diagonal long-range order (ODLRO) by Yang, is associated with a large eigenvalue in the two-electron reduced density matrix (2-RDM). Unlike bosonic long-range order, which is characterized by a large eigenvalue in the one-electron reduced density matrix (1-RDM), fermionic ODLRO has no classical analog, since the off-diagonal elements of the 2-RDM are non-zero only in the quantum description. Coleman (7; 8) showed that the large eigenvalue of the 2-RDM occurs for finite N-electron systems in the context of N-projected Bardeen-Cooper-Schrieffer (BCS), or antisymmetric geminal power (AGP), wave functions. As a result, the magnitude of the large eigenvalue of the 2-RDM can be used as an indicator of phenomena with ODLRO including superconductivity (9; 10; 11).

Because electrons are indistinguishable with pairwise interactions, the total energy of any molecule or material is a linear functional of the 2-RDM (8; 12). In general, the 2-RDM provides information concerning pair properties of a fermionic system. Diagonal elements give information about the populations of fermion pairs, while off-diagonal elements give information about the correlations between fermion pairs. By unitary transformation, we can obtain the pair probabilities with respect to different set of orbitals including points in

coordinate space. Furthermore, the 2-RDM contains the probability distributions for not only two fermion particle but also one fermion particle and one fermion hole as well as two fermion holes (8; 12; 13). Recent work (14) has proposed that the many-body correlations contained in the 2-RDM are accessible by ultrafast pump-probe experiments, as the probability of a system remaining in the ground state when perturbed in this manner is expressible in terms of the 2-RDM or its connected (cumulant) part.

Cumulants, which were first discussed by Thiele (15) in the 1800s and connected across different areas of physics by Kubo in the 1960s (16), are widely applied in both quantum field theory (17; 18; 19) and quantum chemistry (20; 21; 12). The cumulant expansions of reduced density matrices (RDMs) have been particularly useful in electronic structure where they have been used to remove the indeterminacy of the contracted Schrödinger equation (22; 23; 24; 25; 26; 27). The cumulant 2-RDM has been previously studied as a quantifier of electron correlation and entanglement in both time-independent (28; 29; 30; 31; 14) and time-dependent systems (32). In this paper we examine the cumulant part of the 2-RDM as a measure of ODLRO, which is a special type of correlation and entanglement. While the full 2-RDM scales quadratically with system size, the cumulant 2-RDM scales linearly with system size, making it more appropriate for the study of the extent of ODLRO in finite systems. We show that like the 2-RDM the cumulant part of the 2-RDM also exhibits a large positive eigenvalue in the presence of long-range order. Furthermore, in the limit that the size (rank) of the one-electron basis set approaches infinity, we also find that the largest eigenvalue of the cumulant 2-RDM shares with the largest eigenvalue of the 2-RDM the same upper bound of N. We also find that the trace of the cumulant 2-RDM can reach its extreme value of $-N$ in the presence of ODLRO even though this limiting behavior does not appear to be exclusively associated with ODLRO (33; 34). Unlike the large eigenvalue, the trace of the cumulant 2-RDM depends only upon the 1-RDM, indicating as Coleman (8) had suggested that the 1-RDM contains an imprint of ODLRO.

4.2 Theory

The ensemble N-particle density matrix $D(123..N;\bar{1}\bar{2}\bar{3}..\bar{N})$ can be expressed in terms of a set of N-particle wave functions $\{\Psi_i(123..N)\}$ and nonnegative weights $\{w_i\}$

$$D(123..N;\bar{1}\bar{2}\bar{3}..\bar{N}) = \sum_i w_i \Psi_i(123..N)\Psi_i^*(\bar{1}\bar{2}\bar{3}..\bar{N}), \tag{4.1}$$

where the roman numbers represent the spatial and spin coordinates of each particle. Integrating the N-particle density matrix over all particles save two yields the 2-RDM

$${}^2D(1,2;\bar{1},\bar{2}) = \int D(123..N;\bar{1}\bar{2}3..N)d3..dN. \tag{4.2}$$

Importantly, the coordinates of the 2-RDM can be expanded in terms of a set of one-particle functions (spin orbitals) $\{\phi_i(1)\}$

$${}^2D(12;\bar{1}\bar{2}) = \sum_{i,j,k,l} {}^2D_{kl}^{ij}\phi_i(1)\phi_j(2)\phi_k^*(\bar{1})\phi_l^*(\bar{2}), \tag{4.3}$$

where ${}^2D_{kl}^{ij}$ are the elements of the 2-RDM. Consider the cumulant expansion of the 2-RDM

$${}^2D_{kl}^{ij} = 2\,{}^1D_k^i \wedge {}^1D_l^j + {}^2\Delta_{kl}^{ij}, \tag{4.4}$$

where the Grassmann wedge product (35; 20; 36) is an antisymmetric tensor product

$$2\,{}^1D_k^i \wedge {}^1D_l^j = {}^1D_k^i\,{}^1D_l^j - {}^1D_l^i\,{}^1D_k^j. \tag{4.5}$$

The cumulant (or connected) part of the 2-RDM cannot be written as a wedge product of lower RDMs. We normalize the 2-RDM to have a trace of $N(N-1)$. With these definitions we consider three theorems and two corollaries regarding the large eigenvalue and the trace of the cumulant 2-RDM.

Both Yang (4) and Sasaki (6) showed that the 2-RDM can have an eigenvalue (geminal occupation number) as large as the number N of electrons in the system which is a signature of ODLRO. This maximum occupation occurs for ODLRO in a one-electron basis set of infinite size. Yang and Sasaki's result can be extended to show that the cumulant 2-RDM can have a large eigenvalue, also bounded by N.

Theorem 1: The largest eigenvalue of the cumulant 2-RDM is bounded by N.

Proof: Consider the eigenvector v associated with the largest eigenvalue of the 2-RDM where the number of one-electron basis functions, also known as the rank of the basis set, equals r. Yang and Sasaki (4; 6) showed that

$$\lambda_D = v^\dagger \, {}^2D \, v \leq N. \tag{4.6}$$

It can be shown that the cumulant 2-RDM has the following eigenvalue bound

$$\begin{aligned}
\lambda_\Delta &= v^\dagger \, {}^2\Delta \, v && (4.7)\\
\lambda_\Delta &= v^\dagger \, ({}^2D - 2 \, {}^1D \wedge {}^1D) \, v && (4.8)\\
&= v^\dagger \, {}^2D \, v - 2 v^\dagger ({}^1D \wedge {}^1D) v && (4.9)\\
&= \lambda_D - 2 v^\dagger ({}^1D \wedge {}^1D) v && (4.10)\\
&\leq \lambda_D && (4.11)\\
&\leq N, && (4.12)
\end{aligned}$$

where we have employed the positive semidefiniteness of ${}^1D \wedge {}^1D$, that is

$$v^\dagger ({}^1D \wedge {}^1D) v \geq 0, \tag{4.13}$$

for all v.

Pairing wave functions, known as extreme antisymmetrized geminal power (AGP) (5; 7; 8) or projected Bardeen-Cooper-Schrieffer (BCS) wave functions, that exhibit a large eigenvalue

in the 2-RDM also exhibit a large eigenvalue in the cumulant part of the 2-RDM that is indicative of long-range order.

Theorem 2: For the extreme AGP the eigenvalue λ_D of the 2-RDM and the eigenvalue λ_Δ of its cumulant are related as follows:

$$\lambda_\Delta = \lambda_D - \frac{N^2}{r^2}.$$

Proof: When the 2-RDM and its cumulant are from an extreme AGP, the 1-RDM is a scalar multiple of the identity matrix with a scalar factor equal to the number of electrons divided by the rank N/r

$$^1D = \frac{N}{r}\,^1I. \tag{4.14}$$

Therefore, for the extreme AGP we have

$$\lambda_\Delta = \lambda_D - 2\frac{N^2}{r^2} v^\dagger (^1I \wedge {}^1I) v, \tag{4.15}$$

$$\lambda_\Delta = \lambda_D - \frac{N^2}{r^2}. \tag{4.16}$$

Corollary 1: In the limit that the size of the one-electron basis set approaches infinity, the 2-RDM and the cumulant 2-RDM from an extreme AGP wave function share the same large eigenvalue equal to N.

Proof: The corollary follows immediately from Theorem 2 and Yang and Sasaki's theorem. The contribution of the unconnected part of the 2-RDM to the large eigenvalue of either the 2-RDM or its cumulant part vanishes in the limit that the rank r (or size) of the one-electron basis set approaches infinity.

The large eigenvalue in the cumulant (connected) 2-RDM occurs if the order of the system extends over N electrons, which we refer to as long-range order. Because the cumulant part of the 2-RDM is connected, it scales linearly with the size of the system, and hence, its largest eigenvalue cannot scale faster than linear in the number of N electrons.

Even though the trace of the cumulant 2-RDM is computable from only a knowledge of the 1-RDM (in fact, just the 1-RDM's eigenvalues), it can reflect the emergence of ODLRO in the 2-RDM.

Theorem 3: The trace of the cumulant 2-RDM becomes increasingly negative with the emergence of long-range order. The trace of the cumulant 2-RDM is always non-positive with a lower bound of $-N$

$$-N \leq Tr({}^2\Delta) \leq 0,$$

in the mean-field limit the trace of the cumulant 2-RDM is zero

$$Tr({}^2\Delta_{\mathrm{mf}}) = 0,$$

and in the extreme-AGP limit the trace of the cumulant 2-RDM is

$$Tr({}^2\Delta_{\mathrm{ext}}) = -N(1 - \frac{N}{r}).$$

Proof: In general,

$$\begin{aligned} Tr({}^2\Delta) &= Tr({}^2D^{ij}_{kl}) - 2\,Tr({}^1D^i_k \wedge {}^1D^j_l), && (4.17)\\ Tr({}^2\Delta) &= Tr({}^1D^2) - N. && (4.18) \end{aligned}$$

Because the eigenvalues of the 1-RDM lie between 0 and 1, we have

$$\begin{aligned} 0 &\leq Tr({}^1D(1 - {}^1D)) && (4.19)\\ Tr({}^1D^2) &\leq Tr({}^1D) && (4.20)\\ Tr({}^1D^2) &\leq N. && (4.21) \end{aligned}$$

Furthermore, the trace of the 1-RDM squared is nonnegative

$$Tr(^1D^2) \geq 0. \tag{4.22}$$

Combining Eq. (4.18) with Eqs. (4.21) and (4.22) proves that the trace of the cumulant 2-RDM has a lower bound of $-N$ and an upper bound of 0. Because the trace of the 1-RDM squared can be written as the sum of the 1-RDM's eigenvalues, the trace of the cumulant 2-RDM can also be expressed in terms of the 1-RDM's eigenvalues n_i

$$Tr(^2\Delta) = \sum_i n_i^2 - N. \tag{4.23}$$

In the mean-field limit the trace of the cumulant 2-RDM is zero because the cumulant 2-RDM itself vanishes since the electrons (orbitals) are not correlated, that is they are not statistically dependent. For extreme AGP the trace of the cumulant is given by

$$\begin{aligned} Tr(^2\Delta_{\text{ext}}) &= N(N-1) - 2\frac{N^2}{r^2} Tr(^1I_k^i \wedge {}^1I_l^j), & (4.24)\\ Tr(^2\Delta_{\text{ext}}) &= N(N-1) - \frac{N^2}{r^2} r(r-1), & (4.25)\\ Tr(^2\Delta_{\text{ext}}) &= -N(1-\frac{N}{r}). & (4.26) \end{aligned}$$

Corollary 2: In the limit that the size of the one-electron basis set approaches infinity, the trace of the cumulant 2-RDM from an extreme AGP wave function approaches $-N$

Proof: In the limit that the rank r approaches infinity, it follows from Theorem 3 that the trace of the cumulant approaches $-N$.

4.3 Applications

We explore the large eigenvalue in the cumulant part of the 2-RDM by considering the family of Hamiltonian operators (8)

$$\begin{aligned}\hat{H} = N - (N-2)\sum_i \eta_i (a^\dagger_{i\alpha} a_{i\alpha} + a^\dagger_{i\beta} a_{i\beta}) \\ - \sum_{ij} \xi_i \xi_j^* a^\dagger_{i\alpha} a^\dagger_{i\beta} a_{j\beta} a_{j\alpha},\end{aligned} \tag{4.27}$$

where the η_i are defined in terms of the ξ_i

$$\eta_i = |\xi_i|^2 \tag{4.28}$$

and the ξ_i are the expansion coefficients in the two-electron function (geminal) $g(12)$

$$g(12) = 2\sum_i \xi_i \phi_{i\alpha}(1) \wedge \phi_{i\beta}(2). \tag{4.29}$$

For even N each Hamiltonian in the family has a unique N-electron ground-state AGP wave function

$$\Psi(123...N) = g(12) \wedge g(34) \wedge ... \wedge g((N-1)N), \tag{4.30}$$

that is generated from wedge products of the geminal $g(12)$. When all of the η_i equal one, the ground-state solution is an extreme AGP wave function with maximum ODLRO.

Varying the geminal's expansion coefficients in the above Hamiltonian allows us to examine the onset of pairing and long-range order in a quantum system through the large eigenvalues of both the 2-RDM and its cumulant part. We approximate the mean-field case using a geminal in which $N/2$ of the $\eta_{i,\mathrm{mf}}$ values approach one and $N/2$ approach zero. The extreme case has all of the $\eta_{i,\mathrm{ext}}$ equal to one. We tune between the mean-field case and the

extreme case using an expression for η_i of the form

$$\eta_i = \alpha\eta_{i,\text{ext}} + (1-\alpha)\eta_{i,\text{mf}} \tag{4.31}$$

where α is a real value between zero and one. When α is set to zero, we create a pure mean-field geminal, while setting it to one creates an extreme AGP, allowing us to show how the large eigenvalue detects long-range order by tuning α between these two values.

The maximum possible eigenvalue λ_Δ $(= N)$ of the cumulant 2-RDM occurs when the rank r of the one-electron basis set approaches infinity. In a finite basis set with rank r the maximum λ_Δ, strictly less than N, occurs at half filling when $N = r/2$. When $N < r/2$, there are not enough particles to support the ODLRO at half filling, and when $N > r/2$, there are not enough holes to support the ODLRO at half filling. In the following examples, to make comparisons of the large eigenvalues and traces of the 2-RDM and its cumulant part in a finite basis set, we use half filling to maximize the possible ODLRO.

As a general quantum system of 50 electrons in 100 orbitals is modulated between a mean-field geminal and an extreme AGP, the large eigenvalue λ_Δ of the both the 2-RDM and its cumulant increase sharply with the initial onset of long-range order and begin to plateau when α is approximately 0.3. While only the large eigenvalue λ_Δ of the cumulant is shown in Fig. 4.1, the large eigenvalue λ_D of the full 2-RDM follows essentially the same curve, its values slightly above those of λ_Δ. As α approaches one, the large eigenvalues gradually approach their maximum. The largest eigenvalue λ_Δ can detect even a small amount of long-range order, and thereby, measure the difference between an extreme AGP and a non-extreme AGP system, even a non-extreme AGP system with some degree of long-range order. As the system is tuned from a mean-field case to an extreme AGP, the difference between the large eigenvalue of the 2-RDM and its cumulant is reduced from a relatively large value to a smaller, limiting value. For an extreme AGP where $N = r/2$, the large eigenvalue of the cumulant part λ_Δ is exactly less than the large eigenvalue λ_D of the

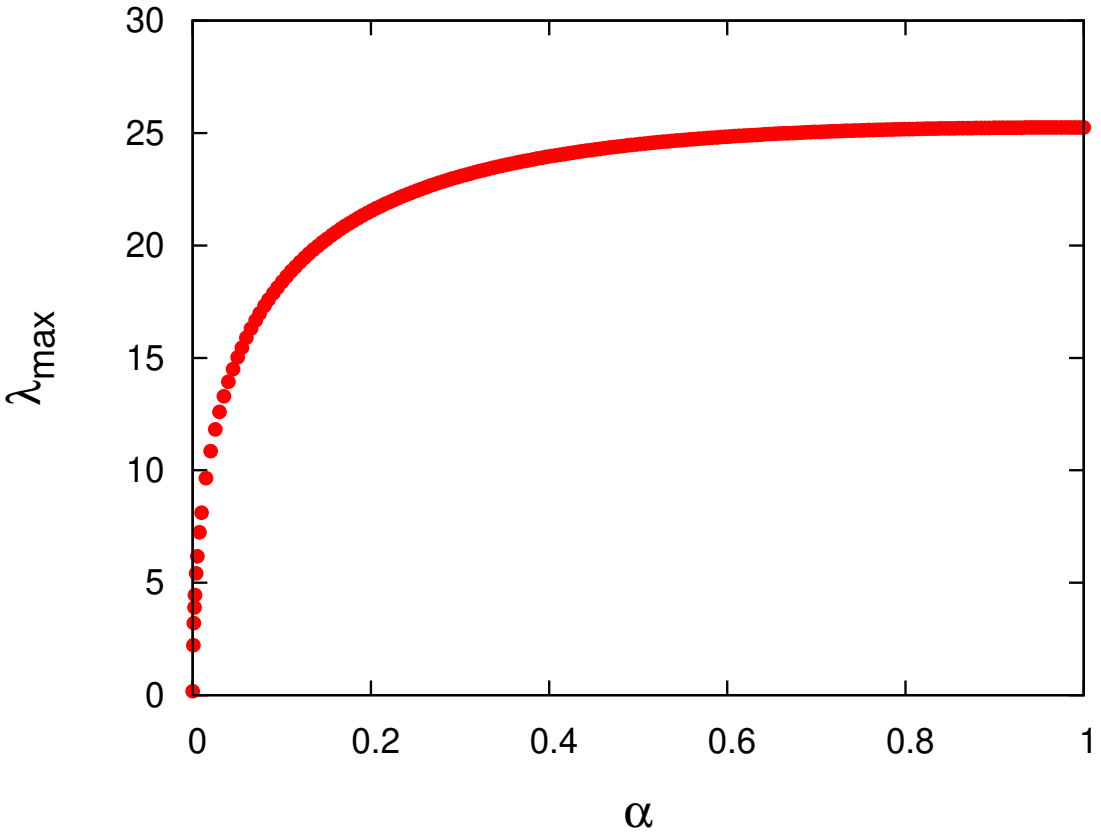

Figure 4.1: The largest eigenvalue of the cumulant part of the 2-RDM is given as a function of α, the tuning parameter, for a general 50-electron, 100-orbital quantum system. As α increases, the eigenvalue captures the emergence of ODLRO.

Table 4.1: Relationships among the large eigenvalue λ_D of the 2-RDM, the large eigenvalue λ_Δ of the cumulant 2-RDM, and the trace of the cumulant 2-RDM are shown as functions of the tuning parameter α for a 50-electron, 100-orbital quantum system. As α increases, all three quantities capture the emergence of ODLRO. The cumulant-derived quantities also vanish in the mean-field limit in the absence of ODLRO.

α	λ_D	λ_Δ	$Tr(^1D)$	$Tr(^2D)$	$Tr(^2\Delta)$
0.0	1.00	0.00	50	4950	0.00
0.1	18.69	18.37	50	4950	-18.12
0.2	21.82	21.53	50	4950	-21.28
0.5	24.76	24.50	50	4950	-24.25
1.0	25.50	25.25	50	4950	-25.00

2-RDM by 1/4

$$\lambda_\Delta = \lambda_D - \frac{1}{4}. \tag{4.32}$$

In addition to the large eigenvalues λ_D and λ_Δ, the increases of this difference $\lambda_\Delta - \lambda_D$ can also be a useful measure of ODLRO with the difference being -1 in the mean-field limit in the absence of ODLRO.

In addition to the large eigenvalue of the cumulant 2-RDM, we show in Table 4.1, for a general quantum system of 50 electrons, that the trace of the cumulant can also reflect the presence of long-range order. Unlike the trace of the 2-RDM, which is constant for a given system of N electrons, the trace of the cumulant decreases with the onset of long-range order, as the geminal is tuned between a mean-field case and an extreme AGP, reaching a minimum value when α is equal to 1. For an extreme AGP when $N = r/2$, the trace of the cumulant part is equal to

$$Tr(^2\Delta) = \frac{1}{2} - \lambda_D. \tag{4.33}$$

The absolute value of the trace follows the same trend as the large eigenvalue of the 2-RDM and the large eigenvalue of the cumulant.

4.4 Discussion and Conclusions

The largest eigenvalue of the cumulant 2-RDM was shown to provide effective measures of off-diagonal long-range order (ODLRO) in quantum many-fermion systems. While Yang and Sasaki (4; 6) previously proved that the largest eigenvalue of the 2-RDM approaches an upper bound of N in the limit of maximum ODLRO, we proved that the largest eigenvalue the cumulant 2-RDM (1) implies the large eigenvalue of the 2-RDM and (2) approaches the same upper bound of N. Unlike the largest eigenvalue of the 2-RDM, the largest eigenvalue of the cumulant 2-RDM vanishes in the absence of ODLRO in the mean-field limit (37). Furthermore, while the 2-RDM has a fixed trace for any system with a fixed number of particles, the variable trace of the cumulant 2-RDM can also reflect the emergence of long-range order. For an extreme AGP wave function in the infinite basis-set limit, the trace of the cumulant 2-RDM reaches its lower bound of $-N$ and thereby reveals maximum ODLRO. While the large eigenvalue of the cumulant 2-RDM implies the large eigenvalue of the 2-RDM, it is also important to note that the trace of the cumulant 2-RDM can also reach its extreme $-N$ value in cases that are not typically associated with ODLRO (see, for example, recent calculations on pairing Hamiltonians (11) and the harmonium model (38; 39)).

Since the development of density functional theory (40), there has been significant interest in how much information is contained within the 1-RDM. The 1-RDM contains significant information about a quantum system's correlation, entanglement, and openness. Recently, a formally complete set of pure N-representability conditions for the 1-RDM, also known as generalized Pauli conditions, have been derived (41; 42) and studied computationally in atoms and molecules (43; 44; 45; 46). The proximity of the 1-RDM to the boundary of its pure N-representable set, or its quasi-pinning to the boundary, is conjectured to place significant restrictions on the correlation and complexity of the wave function. Chakraborty and one of the authors (DAM) (47) have also recently shown that the violation of these conditions by the 1-RDM provides a sufficient condition for the openness of an N-fermion quantum system. In this paper we found that through the trace of the cumulant 2-RDM, which depends

quadratically upon the 1-RDM, the 1-RDM contains an imprint of ODLRO. This result may be useful in improving 1-RDM-based (or geminal-based) energy functionals in electronic structure theory (48; 49; 50; 51). As recent work (52) has experimentally determined the 1-RDM for ultracold fermionic atoms in a double-well potential, the examination of the 1-RDM with respect to ODLRO has the potential to be applied to experimental systems.

Molecules and materials have a plethora of possible energies and properties from the arrangement of atoms in chemical bonds. Special arrangements such as copper-oxide planes have been shown to exhibit extraordinary properties such as high-temperature superconductivity (53). Recent work (54) suggests that ODLRO arises in cuprate and iron-based high temperature superconductors as a result of short-range Coulomb repulsion and long-range attraction between electron pairs in alternating lattice structures. Pairing phenomena in ultracold fermi gases (55), especially in the BCS-BEC limit, are of experimental interest (56; 57; 58; 59) as a method of explaining high temperature superconductivity. The large eigenvalue of the cumulant 2-RDM provides a useful quantity for both quantifying and understanding the presence of ODLRO in quantum molecular systems. While the present results are directly applicable to theoretical and computational studies of long-range order in phenomena like superconductivity, they are also applicable to the study of more general materials with long-range order behavior. Copper oxide compounds, for example, have a high temperature state referred to as a pseudogap metal which has both simple metallic character and long-range quantum entanglement (60). The model Hamiltonians, studied in this paper, show that a continuous curve of largest cumulant 2-RDM eigenvalues can be generated in the range from 0 to N with zero being the mean-field limit and N being the extreme AGP (superconducting) limit. Similarly, materials can have large cumulant 2-RDM eigenvalues that indicate a degree of long-range order between that of a typical insulating material and that of a superconductor. The indicators for ODLRO, developed here, provide new tools for exploring more fully the spectrum of quantum long-range order in molecular systems and materials.

4.5 References

[1] Bardeen, J., Cooper, L. N. & Schrieffer, J. R. Microscopic theory of superconductivity. *Phys. Rev.* **106**, 162 (1957).

[2] Bogoljubov, N. On a new method in the theory of superconductivity. *Nuovo Cim* **7**, 794–805 (1958).

[3] Blatt, J. M. Electron pairs in the theory of superconductivity. *Prog. Theor. Phys.* **23**, 447–450 (1960).

[4] Yang, C. N. Concept of off-diagonal long-range order and the quantum phases of liquid he and of superconductors. *Rev. Mod. Phys.* **34**, 694 (1962).

[5] Coleman, A. J. Structure of fermion density matrices. *Rev. of Mod. Phys.* **35**, 668 (1963).

[6] Sasaki, F. Eigenvalues of fermion density matrices. *Phys. Rev.* **138**, B1338 (1965).

[7] Coleman, A. Structure of fermion density matrices. ii. antisymmetrized geminal powers. *J. Math. Phys.* **6**, 1425–1431 (1965).

[8] Coleman, A. J. & Yukalov, V. I. *Reduced density matrices: Coulson's challenge*, vol. 72 (Springer Science & Business Media, 2000).

[9] Bloch, F. Off-diagonal long-range order and persistent currents in a hollow cylinder. *Phys. Rev.* **137**, A787 (1965).

[10] Erdahl, R. M. & Jin, B. *Many-electron densities and reduced density matrices* (Springer Science & Business Media, 2000).

[11] Rubin, N. C. & Mazziotti, D. A. Strong electron correlation in materials from pair-interacting model hamiltonians. *J. Phys. Chem. C* **119**, 14706–14713 (2015).

[12] Mazziotti, D. A. (ed.) *Reduced-density-matrix mechanics: with application to many-electron atoms and molecules*, vol. 134 (John Wiley & Sons, 2007).

[13] Garrod, C. & Percus, J. K. Reduction of the n-particle variational problem. *J. Math. Phys.* **5**, 1756–1776 (1964).

[14] Pavlyukh, Y. & Berakdar, J. Accessing electronic correlations by half-cycle pulses and time-resolved spectroscopy. *Phys. Rev. A* **90**, 053417 (2014).

[15] Thiele, T. N. *Theory of observations* (Charles & Edwin Layton, 1903).

[16] Kubo, R. Generalized cumulant expansion method. *J. Phys. Soc. Jpn.* **17**, 1100–1120 (1962).

[17] Vladimir, M. & Moskalenko, V. A. Diagram technique for the hubbard model. *Theor. Math. Phys.* **82**, 301–308 (1990).

[18] Negele, J. W. & Orland, H. *Quantum many-particle systems* (Addison-Wesley, 1988).

[19] Foglio, M., Lobo, T. & Figueira, M. General derivation of the green's functions for the atomic approach of the anderson model: application to a single electron transistor (set). *AIP Adv.* **2**, 5225 (2012).

[20] Mazziotti, D. A. Approximate solution for electron correlation through the use of schwinger probes. *Chem. Phys. Lett.* **289**, 419–427 (1998).

[21] Mazziotti, D. A. 3, 5-contracted schrödinger equation: Determining quantum energies and reduced density matrices without wave functions. *Int. J. Quantum Chem.* **70**, 557–570 (1998).

[22] Colmenero, F. & Valdemoro, C. Approximating q-order reduced density matrices in terms of the lower-order ones. ii. applications. *Phys. Rev. A* **47**, 979 (1993).

[23] Nakatsuji, H. & Yasuda, K. Direct determination of the quantum-mechanical density matrix using the density equation. *Phys. Rev. Lett.* **76**, 1039 (1996).

[24] Mazziotti, D. A. Contracted schrödinger equation: Determining quantum energies and two-particle density matrices without wave functions. *Phys. Rev. A* **57**, 4219 (1998).

[25] Mazziotti, D. A. Anti-hermitian contracted schrödinger equation: Direct determination of the two-electron reduced density matrices of many-electron molecules. *Phys. Rev. Lett.* **97**, 143002 (2006).

[26] Snyder Jr, J. W. & Mazziotti, D. A. Photoexcited conversion of gauche-1, 3-butadiene to bicyclobutane via a conical intersection: Energies and reduced density matrices from the anti-hermitian contracted schrödinger equation. *J. Chem. Phys.* **135**, 024107 (2011).

[27] Mazziotti, D. A. Two-electron reduced density matrix as the basic variable in many-electron quantum chemistry and physics. *Chem. Rev.* **112**, 244–262 (2012).

[28] Huang, Z. & Kais, S. Entanglement as measure of electron–electron correlation in quantum chemistry calculations. *Chem. Phys. Lett.* **413**, 1–5 (2005).

[29] Juhász, T. & Mazziotti, D. A. The cumulant two-particle reduced density matrix as a measure of electron correlation and entanglement. *J. Chem. Phys.* **125**, 174105 (2006).

[30] Alcoba, D. R., Bochicchio, R. C., Lain, L. & Torre, A. On the measure of electron correlation and entanglement in quantum chemistry based on the cumulant of the second-order reduced density matrix. *J. Chem. Phys.* **133**, 144104 (2010).

[31] Ramos-Cordoba, E., Salvador, P., Piris, M. & Matito, E. Two new constraints for the cumulant matrix. *J. Chem. Phys.* **141**, 234101 (2014).

[32] Skolnik, J. T. & Mazziotti, D. A. Cumulant reduced density matrices as measures of statistical dependence and entanglement between electronic quantum domains with application to photosynthetic light harvesting. *Phys. Rev. A* **88**, 032517 (2013).

[33] Cioslowski, J. & Buchowiecki, M. Wigner molecules: Natural orbitals of strongly correlated two-electron harmonium. *J. Chem. Phys.* **125**, 064105 (2006).

[34] Cioslowski, J. One-electron reduced density matrices of strongly correlated harmonium atoms. *J. Chem. Phys.* **142**, 114104 (2015).

[35] Ślebodziński, W. *Exterior forms and their applications*, vol. 52 (Polish Scientific Publishers, 1970).

[36] Valdemoro, C. Approximating the second-order reduced density matrix in terms of the first-order one. *Phys. Rev. A* **45**, 4462 (1992).

[37] Fan, H. & Lloyd, S. Entanglement and off-diagonal long-range order of an η-pairing state. *J. Phys. A: Math. Gen.* **38**, 5285 (2005).

[38] Cioslowski, J., Strasburger, K. & Matito, E. The three-electron harmonium atom: The lowest-energy doublet and quadruplet states. *J. Chem. Phys.* **136**, 194112 (2012).

[39] Cioslowski, J., Strasburger, K. & Matito, E. Benchmark calculations on the lowest-energy singlet, triplet, and quintet states of the four-electron harmonium atom. *J. Chem. Phys.* **141**, 044128 (2014).

[40] Parr, R. G. & Yang, W. *Density-Functional Theory of Atoms and Molecules* (Oxford University Press, 1989).

[41] Klyachko, A. A. Quantum marginal problem and n-representability. In *J. Phys.: Conf. Ser*, vol. 36, 1088 (2006).

[42] Altunbulak, M. & Klyachko, A. The pauli principle revisited. *Commun. Math. Phys.* **282**, 287–322 (2008).

[43] Schilling, C., Gross, D. & Christandl, M. Pinning of fermionic occupation numbers. *Phys. Rev. Lett.* **110**, 040404 (2013).

[44] Benavides-Riveros, C. L., Gracia-Bondía, J. M. & Springborg, M. Quasipinning and entanglement in the lithium isoelectronic series. *Phys. Rev. A* **88**, 022508 (2013).

[45] Chakraborty, R. & Mazziotti, D. A. Generalized pauli conditions on the spectra of one-electron reduced density matrices of atoms and molecules. *Phys. Rev. A* **89**, 042505 (2014).

[46] Benavides-Riveros, C. L. & Springborg, M. Quasipinning and selection rules for excitations in atoms and molecules. *Phys. Rev. A* **92**, 012512 (2015).

[47] Chakraborty, R. & Mazziotti, D. A. Sufficient condition for the openness of a many-electron quantum system from the violation of a generalized pauli exclusion principle. *Phys. Rev. A* **91**, 010101 (2015).

[48] Piris, M. Interacting pairs in natural orbital functional theory. *J. Chem. Phys.* **141**, 044107 (2014).

[49] Appel, H. & Gross, E. Time-dependent natural orbitals and occupation numbers. *EPL (Europhys. Lett.)* **92**, 23001 (2010).

[50] Piris, M., Montero, L. & Cruz, N. The bardeen–cooper–schrieffer approach to electron correlation in the density matrix formalism. *J. Chem. Phys.* **107**, 180–187 (1997).

[51] Mazziotti, D. A. Geminal functional theory: a synthesis of density and density matrix methods. *J. Chem. Phys.* **112**, 10125–10130 (2000).

[52] Murmann, S. *et al.* Two fermions in a double well: Exploring a fundamental building block of the hubbard model. *Phys. Rev. Lett.* **114**, 080402 (2015).

[53] Dunne, L. J. & Brändas, E. J. Superconductivity from repulsive electronic correlations on alternant cuprate and iron-based lattices. *Int. J. Quantum Chem.* **113**, 2053–2059 (2013).

[54] Dunne, L. J. High-temperature superconductivity and long-range order in strongly correlated electronic systems. *Int. J. Quantum Chem.* **115**, 1443–1458 (2015).

[55] Pethick, C. J. & Smith, H. *Bose–Einstein condensation in dilute gases* (Cambridge university press, 2008).

[56] Bloch, I., Dalibard, J. & Zwerger, W. Many-body physics with ultracold gases. *Rev.Mod. Phys.* **80**, 885 (2008).

[57] Feld, M., Fröhlich, B., Vogt, E., Koschorreck, M. & Köhl, M. Observation of a pairing pseudogap in a two-dimensional fermi gas. *Nature* **480**, 75–78 (2011).

[58] Lingham, F. K. H. S., MG & Vale, C. Local observation of pair condensation in a fermi gas at unitarity. *Phys. Rev. Lett.* **112**, 100404 (2014).

[59] Okazaki, K. *et al.* Superconductivity in an electron band just above the fermi level: possible route to bcs-bec superconductivity. *Sci. Rep.* **4**, 1–6 (2014).

[60] Punk, M., Allais, A. & Sachdev, S. Quantum dimer model for the pseudogap metal. *Proc. Natl. Acad. Sci. USA* **112**, 9552–9557 (2015).

CHAPTER 5

SIGNATURE OF VAN DER WAALS INTERACTIONS IN THE CUMULANT DENSITY MATRIX

Reprint with permission from O. Werba, A. Raeber, K. Head-Marsden and D. A. Mazziotti, *Phys. Chem. Chem. Phys.* **43** 23900 (2019).

5.1 Introduction

Van der Waals forces are universally experienced by any two molecules. This ubiquity makes them of utmost importance, as seen in their prevalence from microscopic systems involving protein interactions to macroscopic bodies exhibiting adhesion (1; 2; 3; 4). However, computing van der Waals forces and measuring their signature is particularly challenging (5). This is due to the short-range impact of the forces, the fast decay rate of the energy, which is r^{-6} where r is the internuclear separation, and most importantly, their origin in intermolecular electron correlation (6).

Here we propose a density-based approach to measuring and studying van der Waals interactions by using of the cumulant of the two-electron reduced density matrix (2-RDM) (7; 8). Recent work by Via-Nadal, Rodríguez-Mayorga, and Matito (6) has shown that van der Waals forces can be detected in the intracule of the pair density. We extend this approach by using the cumulant part of the 2-RDM which includes the connected part of the pair density as well as additional information. Because van der Waals forces arise from the interaction of induced dipoles, the forces arise from intermolecular electron correlation. The participating electrons on each moiety are statistically dependent on each other, and consequently, the van der Waals forces are contained in the part of the 2-RDM in which the two electrons are statistically dependent, known as the cumulant (or connected) part of the 2-RDM (7; 8; 9; 10). The van der Waals forces are not describable with a mean-field method or a traditional density functional method (11).

To obtain a signature of the van der Waals interaction, we consider the squared Frobenius norm of the cumulant, the trace of the squared cumulant (12; 13; 14). The squared Frobenius norm of the cumulant, which is nonnegative and size extensive, meaning that it scales linearly with system size, has been used as a measure of electron correlation and electron entanglement between different chemical domains. Here, we use the squared Frobenius norm to detect the electron entanglement between the two molecular moieties experiencing the van der Waals interaction. Because the squared Frobenius norm is size extensive, we can use its deviation from its value at infinite separation to measure the electron correlation associated with the interaction. We show that in the presence of van der Waals interactions the square Frobenius norm exhibits an r^{-6} decay with the distance r between two molecules. This density-based analysis provides a fundamental, correlation-driven perspective on the nature of the van der Waals forces. Applications of the cumulant norm are made to a selection of small atoms and molecules to demonstrate the utility of the norm as a detector and quantifier of van der Waals interactions.

5.2 Theory

5.2.1 Cumulant of the 2-RDM

To treat van der Waals forces, we begin with a general construction of the 2-RDM and its cumulant part. Integrating the N-electron density matrix over all electrons save two yields the 2-RDM

$$^2D(1,2;\bar{1},\bar{2}) = \int D(123..N;\bar{1}\bar{2}3..N)d3..dN, \tag{5.1}$$

which describes the probability distribution of two electrons in the field of the remaining N electrons (15; 16; 17; 18). One- and two-electron properties of the electronic system are captured by the 2-RDM because electrons are indistinguishable with pairwise interactions (18). The 2-RDM can be described mathematically as the sum of the wedge product between one-electron reduced density matrices (1-RDMs), ^1D, and a cumulant term, $^2\Delta^{jk}_{kl}$, (12; 13;

8; 9; 19; 15; 16; 20; 21; 22; 23; 24)

$$^2D^{jk}_{kl} = 2\,^1D^i_k \wedge {}^1D^j_l + {}^2\Delta^{jk}_{kl}, \tag{5.2}$$

where the 2-RDM is normalized to $N(N-1)$ and the Grassmann wedge product (25; 7; 26) is an antisymmetric tensor product

$$2\,{}^1D^i_k \wedge {}^1D^j_l = {}^1D^i_k\,{}^1D^j_l - {}^1D^i_l\,{}^1D^j_k. \tag{5.3}$$

This cumulant (or connected) term is the part of the 2-RDM that cannot be written as a wedge product of lower RDMs (7; 27). Because the cumulant term is the part of the 2-RDM in which the two electrons are statistically dependent, it scales linearly with the size of the molecular system (size extensive). The cumulant 2-RDM's size extensivity formally follows from its derivation from an exponential generating functional (7). Reconstruction of the 3- and 4-RDMs in terms of the cumulant 2-RDM has been used in electronic structure methods like the contracted Schrodinger equation method, (28; 29) the anti-Hermitian contracted Schrodinger equation method, (30; 31; 32) canonical transformation, (33) the parametric 2-RDM method, (34; 35) driven-similarity renormalization group, (36) and density cumulant functional theory (37; 38).

The squared Frobenius norm of the cumulant 2-RDM

$$||{}^2\Delta||^2_F = \mathrm{Tr}[({}^2\Delta)^2], \tag{5.4}$$

is a nonnegative, size-extensive quantity that is a useful measure of electron correlation and entanglement (12; 13). In a pure-state quantum system the squared Frobenius norm of the cumulant is nonzero if and only if the system is not correlated. Because the cumulant norm is sensitive to the correlation of electrons (orbitals) on two separated molecules, it can serve as a measure of the electron entanglement of the molecules. When the two molecules are

infinitely separated and not spin entangled, the squared Frobenius norm will equal the sum of each molecules's squared Frobenius norm. The change in the Frobenius norm as the separation between the molecules decreases reflects the intermolecular entanglement of the electrons, which is the quantum-mechanical origin of the intermolecular force or potential.

5.2.2 Measures of van der Waals interactions

The cumulant's squared Frobenius norm can be applied to detect and quantify intermolecular forces. While the change in the energy with distance gauges the intermolecular potential's contribution to the potential energy surface, the cumulant norm reflects the entanglement of the electrons across the molecules that generates the intermolecular potential. Recent work by Via-Nadal, Rodríguez-Mayorga, and Matito (6) has established that the signature of the van der Waals interactions can be calculated for H and He based on the intracule pair density, which decays at a rate of r^{-3}. Here we employ the cumulant 2-RDM and its squared Frobenius norm rather than the correlated part of the intracule pair density to study these interactions. A potential computational advantage of the cumulant 2-RDM is that can be used to detect the van der Waals forces in any representation—position, momentum, or otherwise. While the cumulant 2-RDM's norm is invariant to one-electron unitary transformations, (39) its diagonal part, such as the correlated pair density in the position representation, is not invariant.

The distance dependence of the cumulant 2-RDM for van der Waals forces can be estimated from: (1) the scaling of the van der Waals energy with respect to distance and (2) the scaling of the effective van der Waals Hamiltonian with respect to distance. It is well-known that the energy of the van der Waals potential scales as r^{-6} and that the effective van der Waals Hamiltonian scales as r^{-3} (40). The electronic energy is expressible in 2-RDM theory as

$$E = \mathrm{Tr}({}^2K^2D), \tag{5.5}$$

where ${}^2K$ is the two-electron reduced Hamiltonian containing the one-electron and two-electron molecular integrals. If we replace the ${}^2K$ by an effective two-electron reduced Hamiltonian for the van der Waals interactions ${}^2K_{\mathrm{vdW}}$ and the ${}^2D$ by its cumulant part ${}^2\Delta$, we obtain a theoretical expression for the van der Waals energy

$$E_{\mathrm{vdW}} \approx \mathrm{Tr}({}^2K_{\mathrm{vdW}}{}^2\Delta). \tag{5.6}$$

Because the van der Waals energy and reduced Hamiltonian are known to scale as r^{-6} and r^{-3} respectively, we have that the cumulant 2-RDM scales as r^{-3}. This result is consistent with that obtained for the correlated pair density derived by Matito and co-workers (6). From the definition of the squared Frobenius norm, we have that in the case of van der Waals interactions the squared Frobenius norm of the cumulant 2-RDM scales as r^{-6}.

5.3 Applications

We apply this theory to model van der Waals forces in a variety of small atomic and molecular dimers and compare these results to experimental data. The variety of geometries in these test systems indicates the relevance for this method for more complex systems.

5.3.1 Computational Methodology

All of the 2-RDM calculations were performed using PySCF(41). In particular, the 2-RDMs were computed with the coupled cluster singles-doubles (CCSD) (42) method in a correlation-consistent double-zeta basis set (cc-pVDZ) (43; 44; 45; 46). The 2-RDMs in the molecular-orbital basis set were obtained for dimer separation distances between 4 and 20 Å at 0.5 Å intervals. With these density matrices we computed the cumulant part of the 2-RDM and the associated squared Frobenius norm. We then fit this data to r^{-6}, as this is the asymptotic scaling of the van der Waals force.

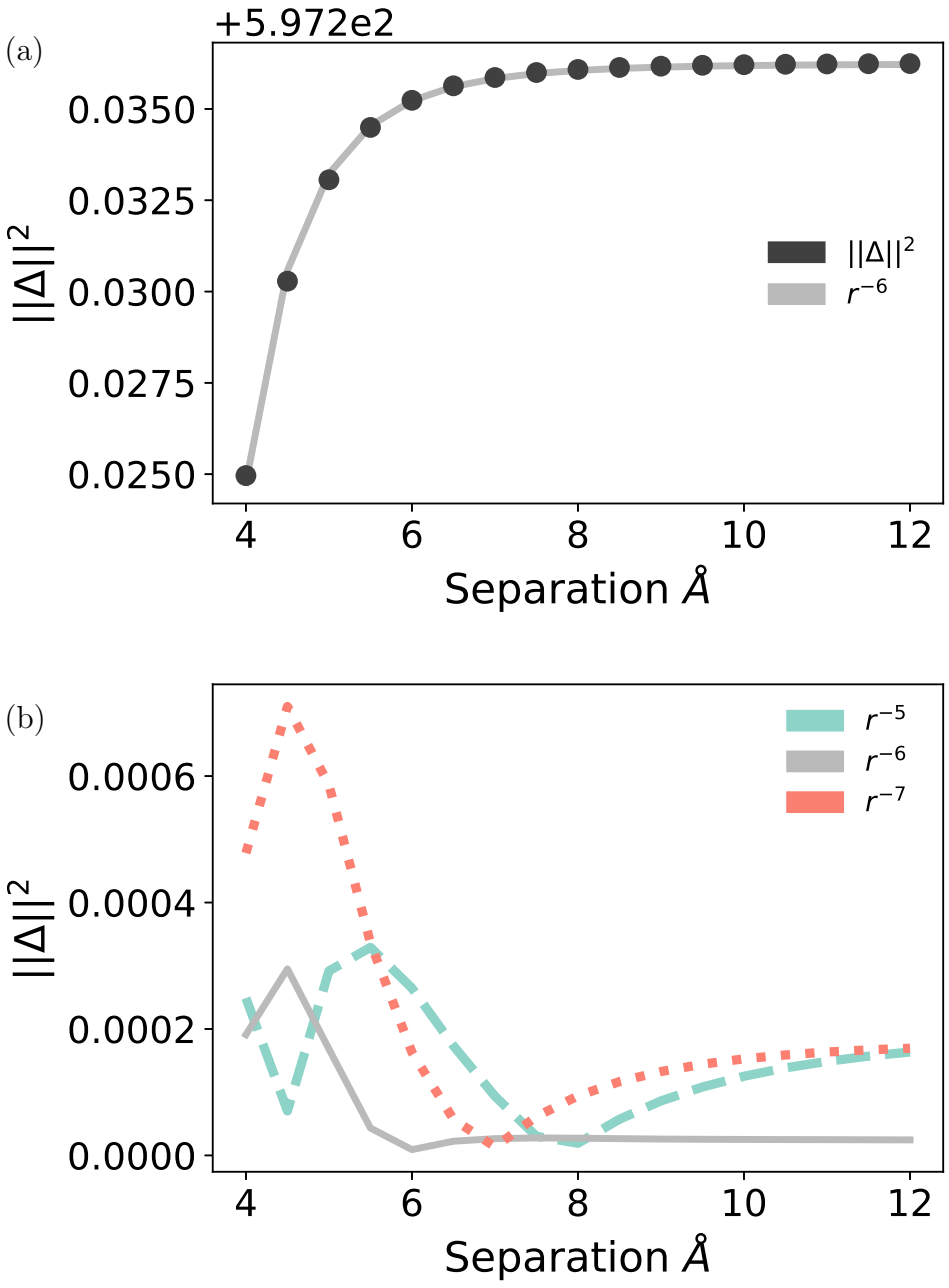

Figure 5.1: In the argon dimer (a) the squared Frobenius of the cumulant 2-RDM as a function of Ar-Ar distance shows the decay of the van der Waals interaction with distance. The black circles indicate the squared Frobenius norm of the cumulant 2-RDM while the solid gray line indicates an r^{-6} function fitted to the squared Frobenius norm. The errors of r^{-5} (teal dashed line), r^{-6} (solid gray line), and r^{-7} (coral dotted line) functions fitted to the squared Frobenius norm of the cumulant 2-RDM reveal in (b) that the data is best approximated by the r^{-6} decay. The $+5.972e2$ denotes a shift of vertical axis's scale.

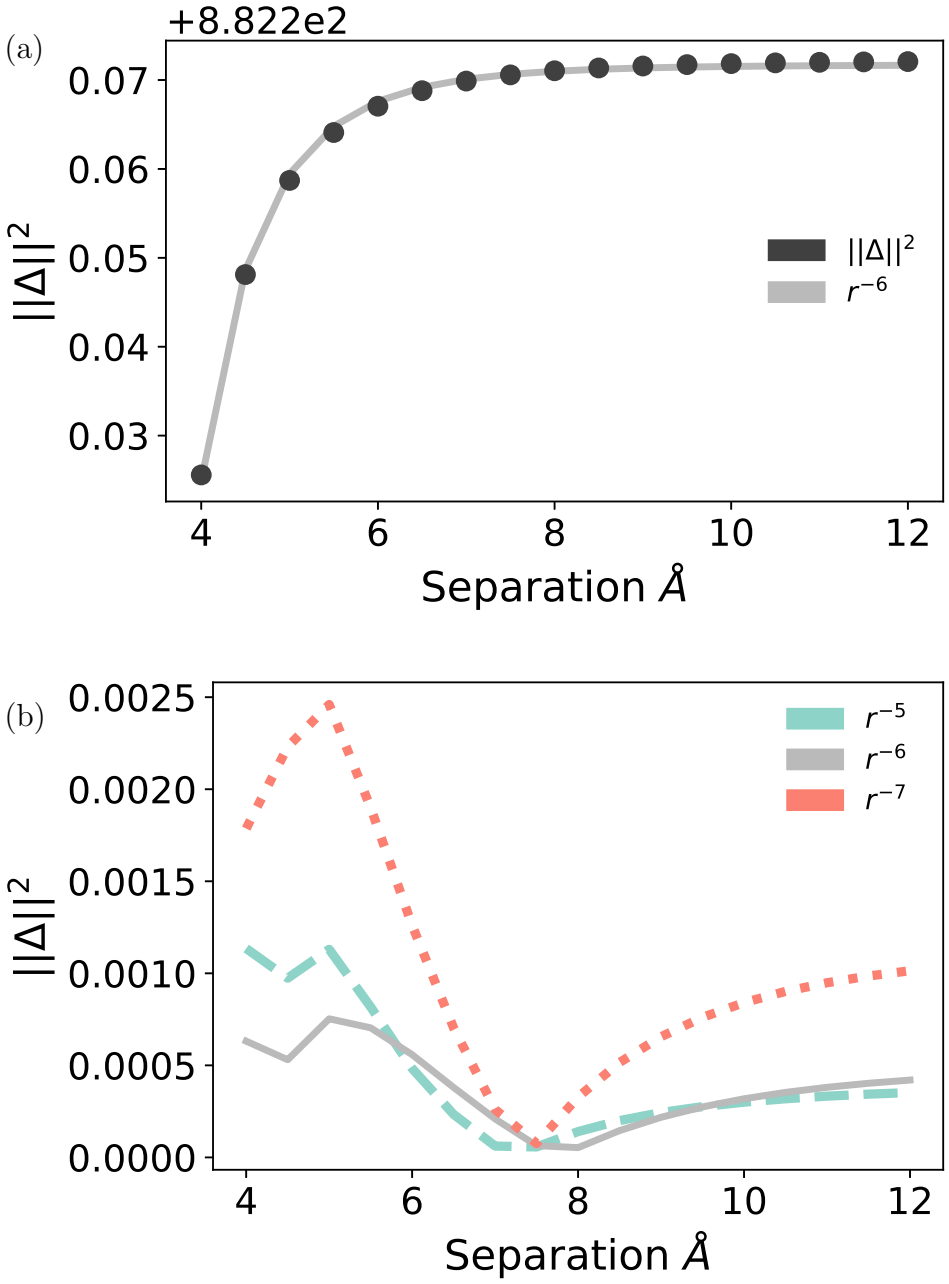

Figure 5.2: In the carbon dioxide dimer (a) the squared Frobenius of the cumulant 2-RDM as a function of the intermolecular distance shows the decay of the van der Waals interaction with distance. The black circles indicate the squared Frobenius norm of the cumulant 2-RDM while the solid gray line indicates an r^{-6} function fitted to the squared Frobenius norm. The errors of r^{-5} (teal dashed line), r^{-6} (solid gray line), and r^{-7} (coral dotted line) functions fitted to the squared Frobenius norm of the cumulant 2-RDM reveal in (b) that the data is best approximated by the r^{-6} decay. The $+8.822e2$ denotes a shift of vertical axis's scale.

5.3.2 Results

First, we consider the classic, isotropic van der Waals interactions in the argon noble gas dimer. As shown in Fig. 1a, the squared Frobenius norm of the cumulant increases and then plateaus as the argon atoms are separated in the range of 4 Å to 12 Å. The Frobenius norm plateaus at a finite, non-zero value that reflects the electron correlation within each of the argon atoms. The decrease in the norm as the atoms are brought together is due to the electron correlation between the argon atoms which gives rise to the van der Waals forces. The circles in the plot represent computed Frobenius norms while the solid line denotes an $\alpha/r^{-6} + \beta$ least-squares fit. As expected from the theory, we find that the r^{-6} fit is highly accurate. For comparison, we show the errors from r^{-5}, r^{-6}, and r^{-7} least-squares fits in Fig. 1b. Results confirm that the data has an r^{-6} asymptotic decay.

There is also high agreement between the data of the cumulant 2-RDM's squared Frobenius norm and the r^{-6} decay for the anisotropic interaction of the carbon dioxide dimer, as seen in Fig. 2a. This dimer was in a parallel geometry, pulled apart from the carbon centers.Inspection of Fig. 2b indicates the preference of the r^{-6} fit, relative to similar fits for r^{-5} and r^{-7}, in capturing the system behavior for a larger variety of distances. This indicates the potential scope of this method, as it captures the electronic interactions of molecular dimers of differing geometries and sizes. The success of the method for molecules with a variety of orientations suggests its potential utility for larger, biological systems.

In order to make this relationship explicit, the R^2 values for these fits are tabulated in Table 5.1. As is evident from this table, the dimer systems universally achieved highest accuracy fitting results with decays of $C_6 r^{-6}$, where C_6 is a density-based van der Waals coefficient. This indicates the validity of the squared Frobenius norm of the cumulant 2-RDM as a measure of the van der Waals signature, which decays at a rate of r^{-6}. This relationship holds for small molecules with a variety of geometries, suggesting the versatility of the approach.

Moreover, it is possible to compare loosely the density-based C_6 values from the fitting

Table 5.1: The R^2 value for fitting the square of the cumulant 2-RDM's Frobenius norm of each of the following molecules to the decay functions r^{-5}, r^{-6}, and r^{-7} are shown, indicating that the computed data is consistent with the predicted r^{-6} decay.

	R^2		
Molecule	r^{-5}	r^{-6}	r^{-7}
F_2-F_2	.989	.999	.987
Ar-SO_2	.986	.999	.997
BH_3-BH_3	.987	.999	.996
Ar-CO_2	.988	.999	.987
Ar-Ar	.995	.999	.990
CH_4-CH_4	.983	.997	.994
NH_3-NH_3	.991	.996	.988
Be-Be	.991	.999	.963
CO_2-CO_2	.997	.998	.997
SO_2-SO_2	.983	.997	.994

Table 5.2: Comparison of the calculated density-based C_6 values with the energy-based C_6 literature values

Molecule	Computed $\lvert C_6\rvert$	Literature $\lvert C_6\rvert$[a]
F_2-F_2	9.39	-
Ar-SO_2	23.2	-
BH_3-BH_3	43.6	-
Ar-CO_2	17.7	114.5
Ar-Ar	47.0	64.4
CH_4-CH_4	63.3	130
NH_3-NH_3	84.9	89.0
Be-Be	188	214
CO_2-CO_2	193	159
SO_2-SO_2	557	294

[a] References for Ar-CO_2 (47), Ar(48), CH_4 (49), NH_3 (50), Be (51), CO_2 (52), SO_2 (53), as tabulated by Vydrov and Van Voorhis (54)

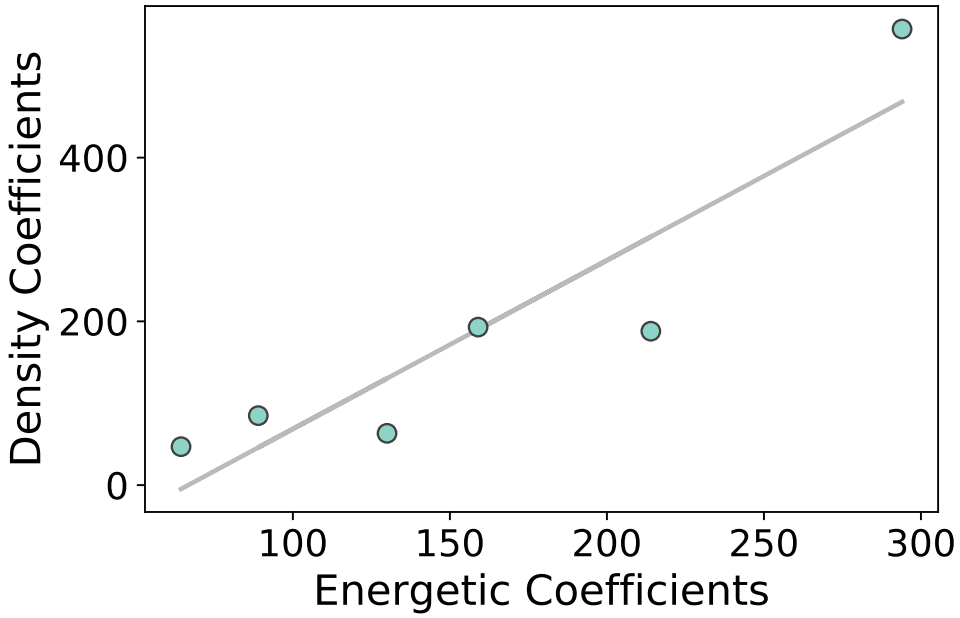

Figure 5.3: Linear regression of the calculated density C6 coefficients versus the literature energetic C6 coefficients is shown.

with the energy-based literature values. This comparison is tabulated in Table 5.2. We do see discrepancies in the resulting data when comparing the energy- and density-based results due to significant differences in the two quantities. The van der Waals forces can in principle affect the cumulant 2-RDM norm more or less than the energy. The energy is weighting the change in the cumulant 2-RDM through its trace with the two-electron reduced Hamiltonian matrix.

Visually, we can see the coherence between the trends in the two methods in the linear regression shown in Fig. 3. This model has an R^2 value of 0.84, indicating consistency between the trends in the literature and the trends in our data. This agreement suggests validity in the data, as it is impossible to compare the values explicitly due to the difference between the decay of the intermolecular energies and the decay of the intermolecular part of the cumulant density matrix.

5.4 Discussion and Conclusions

In this paper we propose and implement a universal signature of the van der Waals interactions based on the cumulant part of the two-electron reduced density matrix (2-RDM). The cumulant is the connected part of the 2-RDM (7; 8) which is not only size extensive and but also invariant to unitary transformations of the orbitals (39). This invariance extends recent work by Via-Nadal, Rodríguez-Mayorga, and Matito (6) who examined the use of the pair density to detect van der Waals interactions. Previously, Juhász and Mazziotti (13; 12) showed that the squared Frobenius norm of the cumulant provides a size extensive measure of electron correlation and entanglement. Here we apply this cumulant norm to quantify the electron entanglement between molecules that gives rise to the van de Waals attraction. Like the energy, we show that the cumulant norm has an r^{-6} decay with respect to molecular separation. The cumulant-based signature of van der Waals forces provides a direct measure of the entanglement of electrons on the separated molecules that is responsible for the van der Waals potential.

Computations with a selection of small molecules confirm the r^{-6} decay of the squared Frobenius norm of the cumulant with respect to molecular separation. These results also imply that the cumulant 2-RDM has a r^{-3} decay which is consistent with the theoretical result presented earlier in the paper. The density-based signature for van der Waals forces provides a systematic approach to quantifying these forces as well as connecting them to the underlying electron entanglement between the molecules. Many electronic structure methods such as conventional density functional theory have difficulty capturing the r^{-6} decay of van der Waals forces with molecular separation (5; 55). These difficulties arise from an incorrect description of the electron correlation. The description of van der Waals forces in terms of the cumulant 2-RDM provides greater understanding of the inner workings of these forces but also a mechanism for assessing their description by various electronic structure methods.

5.5 References

[1] N. Israelachvili, J. The nature of van der Waals forces. *Contemp. Phys.* **15**, 159–178 (1974).

[2] Autumn, K. *et al.* Adhesive force of a single gecko foot-hair. *Nature* **405**, 681–685 (2000).

[3] Sutter, P., Wimer, S. & Sutter, E. Chiral twisted van der Waals nanowires. *Nature* (2019).

[4] DelRio, F. W. *et al.* The role of van der Waals forces in adhesion of micromachined surfaces. *Nat. Mater.* **4**, 629–634 (2005).

[5] Dobson, J. F. *et al.* Prediction of dispersion forces: Is there a problem? *Aust. J. Chem.* 513 (2001).

[6] Via-Nadal, M., Rodríguez-Mayorga, M. & Matito, E. Salient signature of van der Waals interactions. *Phys. Rev. A* **96**, 050501 (2017).

[7] Mazziotti, D. A. Contracted Schrödinger equation: Determining quantum energies and two-particle density matrices without wave functions. *Chem. Phys. Lett.* **289**, 419 (1998).

[8] Mazziotti, D. A. 3,5-contracted Schrödinger equation: Determining quantum energies and reduced density matrices without wave functions. *Int. J. Quantum Chem.* **70**, 557–570 (1998).

[9] Mazziotti, D. A. *Contracted Schrödinger Equation*, chap. 8, 165–203 (John Wiley & Sons, Ltd, 2007).

[10] Benavides-Riveros, C. L., Lathiotakis, N. N., Schilling, C. & Marques, M. A. L. Relating correlation measures: The importance of the energy gap. *Phys. Rev. A* **95**, 032507 (2017).

[11] Parr, R. & Yang, W. *Density-Functional Theory of Atoms and Molecules*. International Series of Monographs on Chemistry (Oxford University Press, USA, 1994).

[12] Skolnik, J. T. & Mazziotti, D. A. Cumulant reduced density matrices as measures of statistical dependence and entanglement between electronic quantum domains with application to photosynthetic light harvesting. *Phys. Rev. A* **88**, 032517 (2013).

[13] Juhász, T. & Mazziotti, D. A. The cumulant two-particle reduced density matrix as a measure of electron correlation and entanglement. *J. Chem. Phys.* **125**, 174105 (2006).

[14] Alcoba, D. R., Bochicchio, R. C., Lain, L. & Torre, A. On the measure of electron correlation and entanglement in quantum chemistry based on the cumulant of the second-order reduced density matrix. *J. Chem. Phys.* **133**, 144104 (2010).

[15] Coleman, A. J. Structure of fermion density matrices. *Rev. Mod. Phys.* **35**, 668–686 (1963).

[16] Coleman, A. & Yukalov, V. *Reduced Density Matrices: Coulson's Challenge* (Springer, 2000).

[17] Mazziotti, D. Structure of fermionic density matrices: Complete n-representability conditions. *Phys. Rev. Lett.* **108**, 263002 (2012).

[18] Mazziotti, D. A. *Reduced-Density-Matrix Mechanics: With Application to Many-Electron Atoms and Molecules*, vol. 134 (John Wiley & Sons, Inc., 2007).

[19] Mazziotti, D. A. Comparison of contracted Schrödinger and coupled-cluster theories. *Phys. Rev. A* **60**, 4396–4408 (1999).

[20] Garrod, C. & Percus, J. Reduction of the n-particle variational problem. *J. Math. Phys.* **5**, 1756–1776 (1964).

[21] McWeeny, R. Some recent advances in density matrix theory. *Rev. Mod. Phys.* **32**, 335–369 (1960).

[22] Kutzelnigg, W. & Mukherjee, D. Cumulant expansion of the reduced density matrices. *J. Chem. Phys.* **110**, 2800–2809 (1999).

[23] Kong, L. & Valeev, E. F. A novel interpretation of reduced density matrix and cumulant for electronic structure theories. *J. Chem. Phys.* **134**, 214109 (2011).

[24] Hanauer, M. & Köhn, A. Communication: Restoring full size extensivity in internally contracted multireference coupled cluster theory. *J. Chem. Phys.* **137**, 131103 (2012).

[25] Slebodziski, W. *Exterior Forms and their Applications* (Polish Scientific Publishers, 2002).

[26] Valdemoro, C. Approximating the second-order reduced density matrix in terms of the first-order one. *Phys. Rev. A* **45**, 4462 (1992).

[27] Raeber, A. & Mazziotti, D. A. Large eigenvalue of the cumulant part of the two-electron reduced density matrix as a measure of off-diagonal long-range order. *Phys. Rev. A* **92**, 052502 (2015).

[28] Mazziotti, D. A. Contracted Schrödinger equation: Determining quantum energies and two-particle density matrices without wave functions. *Phys. Rev. A* **57**, 4219–4234 (1998).

[29] Mazziotti, D. A. Variational method for solving the contracted Schrödinger equation through a projection of the n-particle power method onto the two-particle space. *J. Chem. Phys.* **116**, 1239–1249 (2002).

[30] Mazziotti, D. A. Anti-Hermitian contracted Schrödinger equation: Direct determination of the two-electron reduced density matrices of many-electron molecules. *Phys. Rev. Lett.* **97**, 143002 (2006).

[31] Mazziotti, D. A. Multireference many-electron correlation energies from two-electron reduced density matrices computed by solving the anti-Hermitian contracted Schrödinger equation. *Phys. Rev. A* **76**, 052502 (2007).

[32] Sand, A. M. & Mazziotti, D. A. Enhanced computational efficiency in the direct determination of the two-electron reduced density matrix from the anti-Hermitian contracted Schrödinger equation with application to ground and excited states of conjugated π-systems. *J. Chem. Phys.* **143**, 134110 (2015).

[33] Yanai, T. & Chan, G. K.-L. Canonical transformation theory for multireference problems. *J. Chem. Phys.* **124**, 194106 (2006).

[34] Mazziotti, D. A. Parametrization of the two-electron reduced density matrix for its direct calculation without the many-electron wave function. *Phys. Rev. Lett.* **101**, 253002 (2008).

[35] Bertels, L. W. & Mazziotti, D. A. Accurate prediction of diradical chemistry from a single-reference density-matrix method: Model application to the bicyclobutane to gauche-1,3-butadiene isomerization. *J. Chem. Phys.* **141**, 044305 (2014).

[36] Evangelista, F. A. A driven similarity renormalization group approach to quantum many-body problems. *J. Chem. Phys.* **141**, 054109 (2014).

[37] Kutzelnigg, W. Density-cumulant functional theory. *J. Chem. Phys.* **125**, 171101 (2006).

[38] Copan, A. V., Sokolov, A. Y. & Schaefer, H. F. Benchmark study of density cumulant functional theory: Thermochemistry and kinetics. *J. Chem. Theory Comput.* **10**, 2389–2398 (2014).

[39] Benayoun, M. D., Lu, A. & Mazziotti, D. A. Invariance of the cumulant expansion under 1-particle unitary transformations in reduced density matrix theory. *Chem. Phys. Lett.* **387**, 485 – 489 (2004).

[40] Karplus, M. & Porter, R. N. *Atoms and Molecules* (New York, W. A. Benjamin, 1970).

[41] Sun, Q. *et al.* Pyscf: the python-based simulations of chemistry framework. *Wiley Interdisciplinary Reviews: Computational Molecular Science* **8**, e1340 (2018).

[42] Purvis, G. D. & Bartlett, R. J. A full coupled-cluster singles and doubles model: The inclusion of disconnected triples. *J. Chem. Phys.* **76**, 1910–1918 (1982).

[43] Purvis, G. D. & Bartlett, R. J. A full coupled-cluster singles and doubles model: The inclusion of disconnected triples. *J. Chem. Phys.* **76**, 1910–1918 (1982).

[44] Moser, R. L. C. *Advances in Chemical Physics*, vol. 14 (John Wiley & Sons, Ltd., 1969).

[45] Scuseria, G. E., Janssen, C. L. & Schaefer, H. F. An efficient reformulation of the closed-shell coupled cluster single and double excitation (CCSD) equations. *J. Chem. Phys.* **89**, 7382–7387 (1988).

[46] Scuseria, G. E. & Schaefer, H. F. Is coupled cluster singles and doubles (CCSD) more computationally intensive than quadratic configuration interaction (qcisd)? *J. Chem. Phys.* **90**, 3700–3703 (1989).

[47] Pack, R. T. van der waals interactions of carbon dioxide. *J. Chem. Phys.* **61**, 2091–2094 (1974).

[48] Kumar, A. & Thakkar, A. J. Dipole oscillator strength distributions with improved high-energy behavior: Dipole sum rules and dispersion coefficients for Ne, Ar, Kr, and Xe revisited. *J. Chem. Phys.* **132**, 074301 (2010).

[49] Thomas, G. F. & Mulder, W. J., Fred Meath. Isotropic C6, C8 and C10 interaction coefficients for CH_4, C_2H_6, C_3H_8, n-C_4H_10 and cyclo-C_3H_6. *Chem. Phys.* **54**, 45 – 54 (1980).

[50] Margoliash, D. J. & Meath, W. J. Pseudospectral dipole oscillator strength distributions and some related two body interaction coefficients for H, He, Li, N, O, H_2, N_2, O_2, NO, N_2O, H_2O, NH_3, and CH_4. *J. Chem. Phys.* **68**, 1426–1431 (1978).

[51] Derevianko, A., Porsev, S. G. & Babb, J. F. Electric dipole polarizabilities at imaginary frequencies for hydrogen, the alkali-metal, alkaline-earth, and noble gas atoms. *At. Data Nucl. Data Tables* **96**, 323 – 331 (2010).

[52] Jhanwar, B. L. & Meath, W. J. Dipole oscillator strength distributions, sums, and dispersion energy coefficients for CO and CO_2. *Chem. Phys.* **67**, 185 – 199 (1982).

[53] Kumar, A. & Meath, W. J. Pseudo-spectral dipole oscillator-strength distributions for SO_2, CS_2 and OCS and values of some related dipole—dipole and triple-dipole dispersion energy constants. *Chem. Phys.* **91**, 411 – 418 (1984).

[54] Vydrov, O. A. & Van Voorhis, T. Dispersion interactions from a local polarizability model. *Phys. Rev. A* **81**, 062708 (2010).

[55] Liu, C.-S., Pilania, G., Wang, C. & Ramprasad, R. How critical are the van der Waals interactions in polymer crystals? *J. Phys. Chem. A* **116**, 9347–9352 (2012).